Computer modelling of B_2O_3. I. New interatomic potentials, crystalline phases and predicted polymorphs

1995 J. Phys.: Condens. Matter 7 8659

(http://iopscience.iop.org/0953-8984/7/46/003)

J. Phys.: Condens. Matter 7 (1995) 8659–8692. Printed in the UK

Computer modelling of B_2O_3: part I. New interatomic potentials, crystalline phases and predicted polymorphs

Akira Takada†‡‖, C R A Catlow† and G D Price§

† Davy Faraday Research Laboratory, Royal Institution of Great Britain, 21 Albemarle Street, London W1X 4BS, UK

‡ Fundamental Research Laboratory, Asahi Glass Co. Ltd, 1150 Hazawa-cho, Yokohama 221, Japan

§ Research School of Geological and Geophysical Sciences, Birkbeck College and University College London Gower Street, London W1E 6BT, UK

Received 1 June 1995

Abstract. Atomistic simulation techniques are applied to the study of crystalline B_2O_3. New interatomic potentials are derived by fitting to *ab initio* energy surfaces derived from both periodic boundary conditions and molecular calculations, to which we add the restraints produced by the observed crystal structures. A novel approach based on linear programming (LP) methodology is used in these fitting procedures. We find that the best potentials have terms which are coordination number dependent. Our potentials are able to reproduce the crystal structures of both polymorphs of B_2O_3. Moreover, we predict the stability of new polymorphs with high boroxol ring contents which may be related to the structures of vitreous phases.

1. Introduction

Boric oxide and borates have a highly complex structural chemistry, and there is a long-standing controversy concerning the structural properties of vitreous B_2O_3 [1]. For this reason there is a strong incentive to develop good procedures for modelling structures and properties of these materials using computational methods. In this paper we focus on the derivation of flexible and transferable interatomic potentials for the modelling of B_2O_3 and borates. Several interatomic potentials have been reported for the study of vitreous structures of B_2O_3. However, no attempts have been made to model the crystal structures of B_2O_3. The approach used in this paper is based on the fact that crystal structures have much information on bonding; moreover, we consider that it is necessary to derive interatomic potentials that reproduce several different crystal structures before proceeding to model vitreous materials, the subject of part 2 of this study.

We first, therefore, describe the background to atomistic simulation techniques and interatomic potential models of the type used in this study, with an emphasis on the difference between them and the quantum-mechanical techniques discussed in companion studies of B_2O_3 [2, 3]. Next, in order to overcome the difficulties in deriving interatomic potentials, a new procedure known as the LP fitting method is developed in which we derive potentials from *ab initio* calculations subject to the restraints provided by the observed crystal structures. The newly derived potentials obtained using this latter method are applied to

‖ Author to whom any correspondence should be addressed.

0953-8984/95/468659+34$19.50

the two crystal structures of B_2O_3 and are then compared with the potentials previously reported for vitreous B_2O_3 by other authors. We use *ab initio* data both from periodic boundary conditions calculations on the crystal structures and from calculations on relevant small molecules. We show that the latter are unable to generate satisfactory potentials for use in modelling crystal structures and properties—a result which has general implications for the use of calculations on small molecules in investigating bonding in ionic and semi-ionic solids. Finally, we apply our potentials to the investigation of the stability of novel polymorphic structures of B_2O_3 which may be closely related to those of the vitreous materials.

2. Atomistic simulation techniques

Computer modelling techniques have made great progress in recent years and are increasingly explaining or predicting the structures and properties of solids [4]. These techniques may be classified into two groups: the first starts from the Schrödinger equation and calculates the electronic structure of the system; the second develops interatomic potentials and applies the resulting potentials to the system under study.

We have recently applied a range of electronic structure techniques to the study of B_2O_3 and borates [2, 3]. These allowed us to model successfully the polymorphs of B_2O_3 and yielded useful information on the nature of the bonding in the materials. However, in modelling complex structures such as vitreous solids, methods based on interatomic potentials are needed. Indeed both lattice statics and dynamics have been extensively used in simulating solids including ionic and semi-ionic materials [4–6]. The success of these methods in modelling structures and properties of perfect and defective solids encourages their application to the challenging structural problems posed by crystalline and amorphous B_2O_3.

3. Interatomic potential models

Many studies have been reported concerning interatomic potentials for oxide materials [5, 6]. We now discuss the functional forms and the methods used to derive appropriate parameters.

3.1. Potential functions

Oxides have been commonly described by the ionic model with formal or partial ionic charges assigned to point entities which also interact via short-range terms. The interactions between point charges arise from the long-range electrostatic (Coulombic) forces between ions, while the short-range interactions come from the overlap of the electron charge clouds of the interacting ions.

The simplest and most widely used short-range form is the central-force pair-potential:

$$V(r_1, r_2, \ldots, r_n) = \sum V_{ij}(|r_i - r_j|). \tag{1}$$

The total potential energy V is summed over all the pair interaction terms, each of which is dependent only on the distance between the ions.

The most widely used function form for pair-potentials for ionic solids is the Buckingham potential:

$$V(r_{ij}) = A_{ij} \exp(-r_{ij}/\rho_{ij}) - C_{ij} r_{ij}^{-6}. \tag{2}$$

The second term is often added to express dispersion and other attractive terms.

Another commonly used functional form, which is considered to be suitable for modelling the effect of covalent bonding is the Morse potential:

$$V(r_{ij}) = D_{ij}\{1 - \exp[-\beta_{ij}(r_{ij} - r_0)]\}^2. \tag{3}$$

Although models using these pair-potentials have reproduced reasonably well not only structures but also properties of oxide materials, more sophisticated models are needed to include polarization or covalent bonding effects more precisely.

Polarizability is described straightforwardly and effectively using the shell model [7] in which an ion is described as comprising a massless shell of charge Y, and a core in which the mass is concentrated; a harmonic spring connects the shell with the core. This model has allowed accurate calculations of dielectric, lattice-dynamical and defect properties of ionic solids [5, 6].

In order to express the directional properties of covalent bonding, a three-body term may be added, the most common of which is the simple- harmonic, bond-bending form:

$$V(\theta) = \tfrac{1}{2}K_B(\theta - \theta_0)^2 \tag{4}$$

where K_B is the bond-bending force constant and θ_0 is the equilibrium bond angle.

For crystalline silicates, simple pair-potential models have been used [8, 9]. But the greatest success has been enjoyed by shell model potentials, including three-body terms [10, 11], which have performed well in modelling the structures and properties of a wide range of crystalline and amorphous materials [4, 6].

3.2. Derivation of interatomic potentials

Interatomic potentials have been derived by two main procedures. The first is the empirical method. The parameters in the potential model are fitted so that they can reproduce the experimental structures and/or properties (e.g. elastic constants, dielectric constants or vibrational properties) as accurately as possible. This method may be applied even when the only data available are the crystallographic parameters, although it is important to use as many data as possible for fitting and testing potential models.

The other approach is to use non-empirical or semi-empirical methods, employing quantum-mechanically calculated data for the relevant potential energy surfaces. In the electron gas method [12], electron densities are calculated for the isolated interacting atoms, and then the Coulomb interactions, the kinetic energy, exchange and correlation contributions to the interaction energy are calculated. *Ab initio* methods are, however, increasingly employed on clusters or periodic arrays of atoms. For example, using the *ab initio*, periodic Hartree–Fock techniques available in the CRYSTAL code, Gale *et al* [13] obtained a potential energy surface to which they fitted a potential which then reproduced the structure and elastic constants of α-Al_2O_3. In the case of cluster calculations, the importance of crystal field effects must be stressed. For example, electron-gas studies commonly introduce the Madelung potential appropriate to the crystal when the wavefunctions are calculated [14]. In addition, we should also note that several *'ab initio'* studies [8, 9] were obliged to use experimental data on elastic constants to determine the partial charge values.

One of the most important aspects concerning a potential model is its transferability. Some potentials successfully reproduce the structures of several polymorphs using the same potentials [8, 15]. Moreover, it has been found that potentials fitted to the crystal structure and properties of SiO_2 when applied to vitreous states yield models which reproduce successfully the experimental RDFs [16]. The degree of transferability of interatomic potentials is, however, commonly a matter of controversy and uncertainty. Careful attention will be paid to this feature in the potentials reported later in this paper.

4. Application of previously reported potentials to crystalline B_2O_3

As noted earlier several potential models have been reported specifically for vitreous B_2O_3 [17–23]. In particular, seven potentials were derived by Verhoef and den Hartog [23] which have more general functional forms. They were modified from the 'V1' potentials of Soules [17, 18] and the 'V5' potential of Xu *et al* [22]. All seven potentials have the same Born–Mayer–Huggins form:

$$V_{ij}(r) = A_{ij}\exp(-r/\rho_{ij}) + q_i q_j e^2/r. \tag{5}$$

The V2 potential was modified from the V1 potential by Verhoef and den Hartog so that correct vibrational frequencies were obtained. The V3 potential had the same pair-potential component as the V2 potential and was supplemented with the O–B–O three-body bond-bending term of the form:

$$V_{ijk}(\theta) = \tfrac{1}{2}K_{ijk}(\theta - \theta_0)^2 \tag{6}$$

where θ_0 is 120° for O–B–O and 130° for B–O–B. The B–O–B three-body term was also added in the V4 potential. In the same manner, the pair-potential parts of the V6 and V7 potentials were modified from the V5 potential to obtain correct frequencies, and the B–O–B three-body term was added to the V7 potential. The potential parameters are given in table 1.

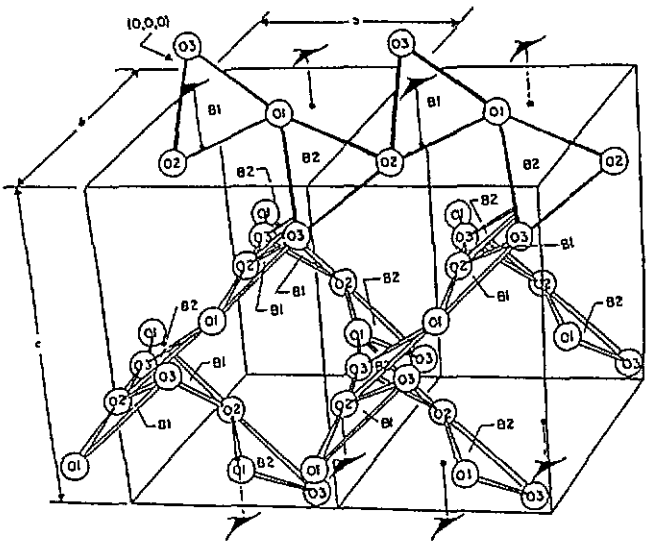

Figure 1. The structure of B_2O_3-I [24].

These potentials do not appear to have been evaluated with respect to their ability to reproduce the properties of the crystalline phases of B_2O_3. We therefore used them in lattice energy minimizations, starting from the experimental structure of B_2O_3-I (figure 1) [24] and B_2O_3-II (figure 2) [25]; for this purpose we employed the GULP code, which can perform a variety of lattice statics (including full minimizations) and dynamics calculations [26]. As the original potentials were not applied to fourfold-coordinated boron atoms, the equilibrium angle θ_0 in the O–B–O three-body interactions is set to be 109.47° in B_2O_3-II. The calculated results are shown in tables 2 and 3. They may be summarized as follows:

(i) For the structure of B_2O_3-I, potentials V4, V5, V6, and V7 reproduce the experimental lattice parameters, B–O bond lengths and O–B–O bond angles reasonably. However, none

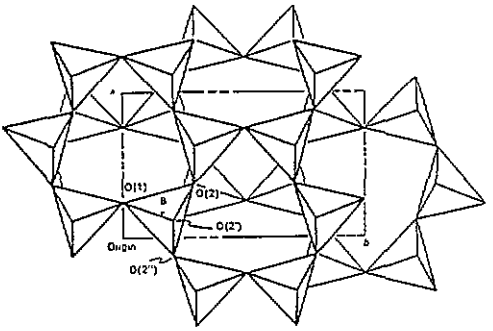

Figure 2. The structure of B_2O_3-II [25].

Table 1. Pair-potential and three-body parameters in the potentials of Verhoef and den Hartog [23]. A_{ij} and ρ_{ij} represent short-range parameters. q_i and K_{j-i-j} represent the charge and bond-bending force constants respectively.

Case	A_{BB}	A_{BO}	A_{OO} (10^3 kJ mol^{-1})	ρ_{BB}	ρ_{BO}	ρ_{OO} (Å)	q_B	q_O	K_{O-B-O}	K_{B-O-B} (kJ rad^{-2})
V1	13.4	78.63	182.3	0.29	0.29	0.29	3.0	−2.0	0	0
V2	9.614	33.72	79.63	0.29	0.29	0.29	2.0	−1.333	0	0
V3	9.614	33.72	79.63	0.29	0.29	0.29	2.0	−1.333	1000	0
V4	6.614	33.72	79.63	0.29	0.29	0.29	2.0	−1.333	1000	500
V5	5.424	1052	149700	0.16	0.165	0.17	3.0	−2.0	0	0
V6	0.6645	128.8	18330	0.16	0.165	0.17	1.050	−0.7	0	0
V7	0.6645	128.8	18330	0.16	0.165	0.17	1.050	−0.7	1500	0

of them can reproduce the B–O–B bond angles. Even for potential V4, which includes the B–O–B three-body term, the B1–O1–B2 angle is still 8° larger than the experimental value. This result explains why the B–O–B bond angles obtained in MD simulations using these potentials were always large. However, the reproduction of the B–O–B bond angles is crucial for correctly describing the manner of connection of the BO_3 triangles—a key feature of the structural chemistry of these materials as discussed later. In this context it is interesting to note that potentials which cannot reproduce the B–O–B bond angles do not predict accurate experimental densities of B_2O_3-I, even if they can reproduce the experimental bond lengths.

(ii) None of the potentials can reproduce the structure of B_2O_3-II, indicating that the bonding for the fourfold-coordinated boron atom is different from that for the threefold-coordinated atoms. Even potential V5, which used in its derivation the crystal structure of the alkaline borate KB_5O_8 which comprises BO_4 tetrahedra, cannot adequately reproduce this structure. The explanation is probably in the difference in the bonding. Indeed we have shown that there is a considerable difference in the ionicity and the nature of the bonding between B_2O_3-II and the alkaline borates [2, 3]. It is interesting to note that these potentials do not lead to the generation of a BO_4-type environment in molten B_2O_3; but the nature of the structural transformation in B_2O_3 may be different from the observed trigonal to tetrahedral conversion of boron on the addition of alkaline oxide. This point will be discussed further in subsequent papers which model the structure of vitreous B_2O_3.

Overall, however, it is clear from the results summarized in this section that previously published potentials have severe deficiencies regarding their ability to reproduce observed

crystal structures of two phases of B_2O_3. Improved models are needed if we are to model vitreous phases of this material.

Table 2. Static lattice simulations of the structure and properties of B_2O_3-I using previously reported potentials [23]. The values in angle brackets were obtained from the experimentally observed structures [24].

	Potential sets for static lattice simulation							
	V1	V2	V3	V4	V5	V6	V7	
(i) Calculated lattice energies in experimental (E1) and energy-minimized (E2) structures (eV/B_2O_3)								
E1	−179.34	−80.40	−80.20	−80.19	−202.26	−24.78	−24.48	
E2	−182.25	−81.70	−81.70	−80.80	−203.91	−24.98	−24.96	
(ii) Energy-minimized structure (ratio with respect to experimental value); unit-cell volume (v), lattice constants (a, b, c) (%)[a]								
v	+79.49	+73.99	+74.12	+6.10	+8.66	+8.64	+6.84	
a	+9.96	+8.84	+8.92	+2.62	+6.12	+6.11	+5.07	
b	+9.96	+9.96	+8.92	+2.62	+6.12	+6.11	+5.07	
c	+48.44	+46.89	+46.78	+0.76	−3.52	−3.52	−3.22	
Bond length (Å)								
B1–O1	1.378	1.364	1.364	1.394	1.348	1.348	1.376	⟨1.404⟩
B1–O2	1.378	1.364	1.364	1.370	1.406	1.406	1.375	⟨1.366⟩
B1–O3	1.372	1.358	1.358	1.383	1.408	1.408	1.408	⟨1.337⟩
B2–O1	1.378	1.364	1.364	1.370	1.406	1 406	1.375	⟨1.336⟩
B2–O2	1.378	1.364	1.364	1.394	1.348	1.348	1.376	⟨1.400⟩
B2–O3	1.372	1.358	1.358	1.383	1.408	1.408	1.408	⟨1.384⟩
Bond angle (deg)								
O1–B1–O2	119.8	119.8	119.9	119.7	120.2	124.1	120.0	⟨119.0⟩
O1–B1–O3	120.1	120.1	120.0	121.4	124.1	124.1	120.4	⟨114.7⟩
O2–B1–O3	120.1	120.1	120.0	118.6	115.4	115.4	119.3	⟨126.1⟩
O1–B2–O2	119.8	119.8	119.9	119.7	120.2	120.2	120.0	⟨121.5⟩
B1–O1–B2	179.1	179.1	179.1	136.6	150.3	150.3	146.0	⟨130.5⟩
B1–O2–B2	179.1	179.1	179.1	136.6	150.3	150.3	146.0	⟨128.3⟩
(iii) Properties for energy-minimized structures								
Elastic constant (GPa)								
E(1, 1)	167.8	77.99	107.4	162.5	183.6	22.5	30.3	
E(1, 2)	71.8	33.0	37.3	45.0	31.7	3.9	−1.1	
Bulk modulus (GPa)								
K	103.8	47.9	60.7	84.2	82.3	10.1	9.4	
Static dielectric constant (experiment: 3.0–3.5)[b]								
$\varepsilon_0(1, 1)$	2.14	2.17	1.90	2.64	2.78	2.78	1.83	
$\varepsilon_0(2, 2)$	2.14	2.17	1.90	2.64	2.78	2.78	1.83	
$\varepsilon_0(3, 3)$	2.12	2.18	1.58	6.40	3.49	3.49	2.53	

[a] Experimental values $v = 135.8$ Å^3, $a = b = 4.336$ Å and $c = 8.340$ Å from [24].
[b] From [27].

5. New potential derivation method (LP fitting method)

5.1. Problems of existing fitting method

We first review the common method for fitting interatomic potentials, as in the widely used codes (THBFIT [28] and GULP) which have been successfully applied to many systems. The general method in such fitting procedures is as follows.

(i) Read in the experimental structures, properties and initial potential parameters.

Table 3. Static lattice simulation of the structure and properties of B_2O_3-II using reported potentials [23]. The values in angle brackets are again from the experimentally observed structure [25].

	Potential sets for static lattice simulation							(Experimental data)
	V1	V2	V3	V4	V5	V6	V7	
(i) Calculated lattice energies in experimental (E1) and energy-minimized (E2) structures (eV/B_2O_3)								
E1	−179.39	−80.39	−80.07	−79.38	−201.36	−24.67	−24.18	
E2	−182.20	−81.67	−80.98	−80.04	−204.71	−25.08	−24.84	
(ii) Energy-minimized structure (ratio with respect to experimental value); unit-cell volume (v), lattice constants (a, b, c) (%)[a]								
v	+ 119.13	+ 116.72	+ 17.82	+ 15.15	+ 30.50	+ 38.48	+ 15.65	
a	+ 29.02	+ 28.98	+ 2.28	+ 2.26	+ 10.13	+ 10.13	+ 3.03	
b	+ 29.02	+ 28.98	+ 2.28	+ 2.26	+ 10.13	+ 10.13	+ 3.03	
c	+ 15.34	+ 14.16	+ 8.27	+ 6.73	+ 8.74	+ 8.74	+ 5.81	
Bond length (Å)								
B1–O1	1.374	1.360	1.360	1.371	1.363	1.363	1.412	⟨1.373⟩
B1–O2	1.378	1.363	1.559	1.538	1.399	1.399	1.546	⟨1.506⟩
B1–O2′	1.363	1.577	1.542	1.399	1.399	1.547	1.508	⟨1.508⟩
B1–O2″	—	—	1.603	1.656	—	—	1.558	⟨1.512⟩
Bond angle (deg)								
O1–B1–O2	120.2	120.2	111.4	108.1	120.9	120.9	110.1	⟨110.2⟩
O1–B1–O2′	120.2	120.2	110.3	112.4	120.9	120.9	110.0	⟨115.8⟩
O1–B1–O2″	—	—	110.0	111.0	—	—	109.9	⟨113.1⟩
O2–B1–O2′	—	—	109.7	110.5	—	—	109.2	⟨107.4⟩
B1–O1–B1	180.0	180.0	164.8	146.1	180.0	180.0	161.2	⟨138.6⟩
B1–O2–B1	180.0	180.0	121.4	118.6	180.0	144.7	121.4	⟨118.7⟩
(iii) Properties for energy-minimized structures								
Elastic constant (GPa)								
$E(1, 1)$	480.6	217.6	418.7	406.2	204.3	250.3	326.8	
$E(1, 2)$	2.6	1.0	57.0	6.3	−42.1	−5.2	46.6	
Bulk modulus (GPa)								
K	161.9	73.2	177.5	139.6	652.9	80.0	140.0	
Static dielectric constant (experiment: 3.0–3.5)[b]								
$\varepsilon_0(1, 1)$	2.13	2.17	2.26	2.02	2.00	2.00	1.44	
$\varepsilon_0(2, 2)$	2.11	2.05	2.29	1.83	3.33	3.33	1.29	
$\varepsilon_0(3, 3)$	2.16	2.20	2.34	1.82	2.71	2.71	1.29	

[a] Experimental values $v = 148.6$ Å^3, $a = 4.613$ Å, $b = 7.803$ Å and $c = 4.129$ Å from [25].
[b] From [27].

(ii) Calculate the cell strains ($\varepsilon(i)$; i = 1–6), internal strains ($\varepsilon_{ij}(i, j)$; i = 1–N, j = 1–3) and properties ($C(i)$; i = 1–m).

(iii) Calculate the weighted square sum of the errors S

$$S = \sum_i w_{1i}\varepsilon(i)^2 + \sum_{ij} w_{2ij}\varepsilon_{ij}(i, j)^2 + \sum_i w_{3i}(C(i) - C_{\text{exp}}(i))^2 \qquad (7)$$

where w_{1i}, w_{2ij} and w_{3i} are weighting factors which control the contribution of each term to S and $C_{\text{exp}}(i)$ are the experimentally observed properties.

(iv) Change the potential parameters in order to reduce the residual S, via a least-squares fitting algorithm.

(v) Iterate from (ii) to (iv) until S is minimized.

This approach can be used for a wide range of fitting problems and the procedure is especially easily applied or refined when there are reasonable initial potential parameters.

However, when this method was applied for B_2O_3 crystals, starting from either reported potential parameters or from modified ones, we did not obtain acceptable potentials. In most cases, the 'best fit' potential still distorts the experimental structure excessively.

The reasons for this problem are as follows.

(i) If an initial parameter set is poor, the least-squares fitting procedure will go to the nearest local minimum which is commonly not the desired solution. One possible solution is to try as many initial sets as possible, but such a procedure may be unreliable or computationally expensive.

(ii) The weighting factors strongly affect S and they easily change the variation of S with the parameters, and may lead to an undesirable local minimum. In the case of a layered system, even if quite small residuals of strain are obtained, they are enough to distort its structure substantially. The other problem is that completely different types of measurements (e.g. structure and properties) are subsumed under S, and it is not always easy to set up the proper weighting factors appropriate for such different data.

(iii) The functional forms of the potentials may be unsuitable, although it is often difficult to show unambiguously that the problems are arising from this factor.

One strategy to overcome these difficulties is to blend *ab initio* methods with empirical fitting [8, 9]. Moreover, effective fitting procedures using this combined approach require a new type of approach as discussed in the next section.

5.2. The linear programming (LP) fitting method

The LP fitting method is designed to fit to *ab initio* surfaces with the added constraint of requiring the reproduction of observed experimental structures. Moreover, the approach is effective in overcoming several of the problems identified in the previous section.

First, regarding the problem of finding the global minimum, if the problem can be linearized, the global minimum can be found within a finite number of iterations. The second point is that separating the criterion of crystal stability from the evaluation of properties can make the fitting problem much easier. It is also desirable that the experimental data (such as the structural stability conditions) should be separated from the *ab initio* potential energy data as components of the cost function. Moreover, when common potentials that can reproduce several different structures at the same time are desired, the introduction of independent sets of structural stability conditions is more reasonable than the use of a unique formula for S. The third point is that it is very helpful to know whether a solution of the problem is feasible, and also which condition obstructs the solution. In particular, it is not clear how well the covalently bonded B_2O_3 system can be described with the existing potential functions.

These ideas lead to new potential fitting method based on the linear programming (LP) method, which is a well-known technique in the field of economics and mathematics [29]. Several special considerations are given in order to adapt the potential fitting problem to the general LP problem as follows.

(i) All the conditions that need to be satisfied are separated into two categories: the first comprises several sets of inequality conditions; the second is a cost function which should be minimized. The fitting procedure essentially involves the determination of the optimum solution that minimizes the cost function within the solution space that satisfies all the inequality relations.

(ii) The conditions of structural stability are defined in the form of inequality relations. Here, the term 'structural stability' means that the relaxed structure does not distort

appreciably from the experimental structure. The lattice energy in the experimental structure is the minimum point in the configurational space ($3N$-dimension) of the energy of the crystal with respect to the coordinates of component ions.

Thus the lattice energy E depends on the atomic coordinates:

$$E = E(x_1, x_2, \ldots, x_n) \tag{8}$$

where the x_i are the position vectors of the ith atom. The equilibrium condition requires therefore:

$$\partial E/\partial x_i = 0 \qquad \partial^2 E/\partial x_i^2 > 0 \tag{9}$$

at the structure of minimum energy ($x_1 = x_{1e}, .., x_n = x_{ne}$). We can therefore write that $\forall \Delta x_i$:

$$E(x_{1e}, x_{2e}, .., x_{ie} + \Delta x_i, .., x_{ne}) > E(x_{1e}, x_{2e}, .., x_{ie}, .., x_{ne}) \tag{10}$$

and

$$E(x_{1e}, x_{2e}, .., x_{ie} - \Delta x_i, .., x_{ne}) > E(x_{1e}, x_{2e}, .., x_{ie}, .., x_{ne}) \tag{11}$$

must be satisfied. When the lattice parameters a, b, c, α, β and γ (6 variables) and the n atomic positions ($n \times 3$ variables) are taken into account, a total of $(6n + 12)$ inequality conditions is generated.

(iii) The weighted sum of the residuals between the *ab initio* data for the potential energy surface and the corresponding calculated values using the present values of the variables of the potential parameters is defined as the cost function. Therefore, the LP method tries to find the solution which achieves the global minimum for the residual within the solution space that satisfies the structural stability conditions. However, there are limitations for the application of the LP method. First, it is not easy to include the evaluation of various physical properties in the cost functions, because within the LP scheme the complex form of such properties must be linearized using the potential parameters. We also note that the cost function must be the linear weighted sum of potential parameters instead of the square weighted sum of them, as in conventional least-squares fitting; although this latter problem poses no severe difficulties.

The most important point of the LP method is that the structural stability conditions are not included in the cost function, but in the inequality relations. Therefore, the merit of this method is that, even if the initial potential functions are poor in describing the structure, the procedure yields a solution which maintains the structure in equilibrium, or it indicates that there is no feasible solution.

(iv) Once the problem is described within the frame of LP, the solution is quickly obtained even by a personal computer. The most significant problem with this method is that the fitting problem must be linearized regarding the potential parameters. Inevitably some parameters (e.g. the ρ parameter in Buckingham form in (2), or the β and r_0 parameters in Morse form in (3)) cannot be linearized simply and must remain fixed as constants during one solution cycle. However, each solution cycle is very quick, allowing a thorough search of a variety of combinations of e.g. ρ or β to be easily performed, in order to find the global minimum.

The algorithm used by the LP fitting method comprises the following stages.

(i) Linearization of each of the terms of which the total lattice energy E is comprised:

$$E = E_c + E_2 + E_3 + E_4 \tag{12}$$

where E_c, E_2, E_3 and E_4 are the contribution of the Coulombic energy, pair-potential, three-body and four-body terms.

For Coulombic terms, they are calculated straightforwardly from the crystal structure and if fixed charges are used, they are dealt with as constants in the inequality relations.

In the case of short-range potentials specified using the Buckingham form:

$$E_2 = \sum_{i>j}\{A_{ij}\exp(-r_{ij}/\rho) - C_{ij}/r_{ij}^6\} = A_{ij}\left\{\sum_{i>j}\exp(-r_{ij}/\rho)\right\} - C_{ij}\left\{\sum_{i>j}1/r_{ij}^6\right\}. \quad (13)$$

The values in the outermost parentheses are calculated only from the crystal structures, and are independent of the unknown variables A and C, when ρ is fixed.

In the case of the Morse form of the short-range potential, we have:

$$E_2 = D_{ij}\left\{\sum_{i>j}[1 - \exp\{-\beta_{ij}(r_{ij} - r_0)\}]^2\right\}. \quad (14)$$

Once more the value in the outermost parenthesis is calculated only from the crystal structures, and is independent of the unknown parameters D_{ij} when β_{ij} and r_0 are fixed.

For the simple harmonic three-body terms,

$$E_3 = K_B \sum_{i>j>k}\{\tfrac{1}{2}(\theta_{ijk} - \theta_0)^2\}. \quad (15)$$

The value in the outermost parenthesis is again calculated only from the crystal structures, and is independent of the unknown parameters K_B when θ_0 is fixed. Four-body terms are dealt with in the same way as the three-body terms.

(ii) Formulation of the inequality conditions for the structural stability condition:

$$E(x_{1e}, .., x_{ie} \pm \Delta x_i, .., x_{ne}) > E(x_{1e}, .., x_{ie}, .., x_{ne}). \quad (16)$$

The coefficients of the unknown variables (A, C, D_{ij} and K_B etc.) are calculated for each structural configuration, and $(6n + 12)$ sets of inequality relations are generated. As an example, we consider one simple model for B_2O_3, which includes the Morse form for the B–O interaction, the Buckingham form for the O–O interactions, and the three-body term for the O–B–O interactions giving therefore four variables (D_{B-O}, A_{O-O}, C_{O-O} and K_{O-B-O}). The lattice energies for an experimental structure and any varied structure can be arranged: for the experimental structure,

$$E_0 = \alpha_{0.1}D_{B-O} + \alpha_{0.2}A_{O-O} - \alpha_{0.3}C_{O-O} + \alpha_{0.4}K_{O-B-O} > 0 \quad (17)$$

for any distorted structure,

$$E_i = \alpha_{i.1}D_{B-O} + \alpha_{i.2}A_{O-O} - \alpha_{i.3}C_{O-O} + \alpha_{i.4}K_{O-B-O} > 0 \quad (18)$$

where the $\alpha_{i.j}$ are calculated only from the crystal structure. Equation (14) provides one inequality relation for its configuration:

$$(\alpha_{i.1} - \alpha_{0.1})D_{B-O} + (\alpha_{i.2} - \alpha_{0.2})A_{O-O} - (\alpha_{i.3} - \alpha_{0.3})C_{O-O} + (\alpha_{i.4} - \alpha_{0.4})K_{O-B-O} > 0. \quad (19)$$

Among all the inequality relations, twelve come from the variations of the cell parameters ($a\Delta \pm a$, $b\Delta \pm b$, $c\Delta \pm c$, $\alpha\Delta \pm \alpha$, $\beta\Delta \pm \beta$, $\gamma\Delta \pm \gamma$), and $6n$ come from the variations of internal coordinates ($x_i\Delta \pm x_i$, $y_i\Delta \pm y_i$, $z_i\Delta \pm z_i$).

(iii) Definition of the cost function S: the deviation between the *ab initio* data on the potential energy surface and the corresponding value estimated from the linearized sum of the parameters are summed up to give the cost function S.

$$S = \sum_i w_i |E_i^{ab} - E_i^{pe}| \tag{20}$$

where w_i is the weighting factor, and E_i^{ab} and E_i^{pe} are the energies derived from the *ab initio* calculations and using the current values of the potential parameters. Usually all the weighting factors are set to 1, and do not need to be changed.

(iv) Addition of the extra inequality conditions if necessary: for example, if the total lattice energy is restricted within some specific range (for example, $E_{min} < E$ and $E < E_{max}$ are given), two inequality relations are added in the same manner as in (ii). It is also very easy to specify the difference of energies between several different structures (for example, when the energy differences ΔE_{12} and ΔE_{23} between three polymorphic structures are given, $E_1 + \Delta E_{12} < E_2$ and $E_2 + \Delta E_{23} < E_3$ are added) .

(v) Application of the general LP algorithm: the coefficients calculated from (i) to (iv) generate the general matrix elements for LP and the variables are solved so that they minimize the cost function S at the finite calculation steps.

(vi) Iteration from (i) to (v), changing the non-linear parts (e.g. ρ, β, or r_0) to yield the solution which locates the global minimum. As many combinations as possible of the unknown parameters are applied systematically.

We may compare this LP fitting method with the other general algorithms as follows. The strengths of the method are first that it is especially suitable for the ill-conditioned problem, where the crystal structure is apt to move toward a catastrophic change (for example, in the case of layered or planar structures). Because the structural stability conditions are absolutely satisfied during the solution, it can always prevent the distortion of its structure. The method is also suitable for the simultaneous fitting of several structures, because all the structural stability conditions are satisfied independently and simultaneously. Secondly, when the linearized coefficients are output, the potential energy surface which depends on the variables (A, C, D_{ij} and K_B) can be easily analysed, because it is simply the linear sum of these terms. In particular, when a satisfactory potential cannot be obtained, it is straightforward to find which stability condition obstructs the solution. Thirdly, the global minimum can be obtained with very modest computer resources. There is no problem about setting the initial conditions or the weighting factors.

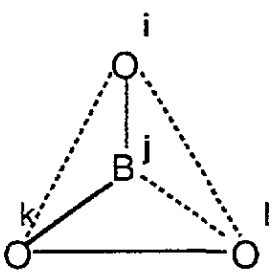

Figure 3. Torsion angle ϕ within the BO_3 triangle, defined as the angle between two planes, each of which is defined by three atoms (i, j, k) and (j, k, l) respectively.

The main weakness of the method is its limited range of applications. The requirement that all the conditions must be linearized is very restrictive. Therefore, features including fitting to crystal properties or the use of the shell model cannot be included at the moment. In such cases it is possible to use the LP fitting procedure as a starting point and to refine the resulting parameters by using more general fitting programs. It is interesting to note that

the LP method is based on linearized optimization with constraints, while the other widely used methods are based on non-linear optimization without constraint. It is likely that, in the future, the two methods will approach each other more closely.

6. Application of the LP fitting method to B_2O_3 crystals

We now apply the new LP fitting method to the derivation of interatomic potentials for B_2O_3 crystals. Our study embraces both B_2O_3-I and B_2O_3-II structures. Two types of *ab initio* calculation are used: first, the periodic boundary conditions Hartree–Fock (HF) methods [30] and secondly calculations on small molecules. Energy surfaces based on the former techniques will be described first.

Table 4. Fitted potentials (A1–A5) based on the B_2O_3-I structure and *ab initio* data.

	Potential sets				
Parameters	A1	A2	A3	A4	A5
Charge					
q(B)	+2.7	+2.7	+2.7	+1.5	+1.2
q(O)	−1.8	−1.8	−1.8	−1.0	−0.8
Morse potential for B–O					
D (eV)	2.580	1.549	1.344	0.466	0.326
β (Å)	2.5	2.7	2.7	2.7	2.7
r_0 (Å)	1.55	1.59	1.59	1.59	1.59
Buckingham potential for O–O					
A (eV)	2229.0	6317.0	5878.0	795.0	727.0
ρ (Å)	0.36	0.35	0.35	0.35	0.35
C (eV Å^6)	0.0	935.2	662.2	60.9	80.9
Buckingham potential for B–B					
A (eV)	0.0	0.0	0.0	0.0	0.0
ρ (Å)	0.35	0.35	0.35	0.35	0.35
C (eV Å^6)	314.9	0.0	456.3	9.1	19.4
Three-body term for O–B–O (θ_0 = 120 for threefold and θ_0 = 109.47 for fourfold coordination)					
k (eV rad^{-2})	0.0	0.0	0.0	0.0	0.0
Three-body term for B–O–B (θ_0 = 120)					
k (eV rad^{-2})	8.08	4.79	—	6.63	2.53
Four-body term for O–B–O–O					
k (eV)	0.85	—	—	—	—

6.1. Potentials based on periodic HF methods

6.1.1. Fitting to B_2O_3-I structure. The experimental structural data of B_2O_3-I are used to obtain the structural stability conditions (thirty-six structural configurations; all lattice constants and internal coordinates are varied), while the *ab initio* potential energy data (eleven structural configurations; see table A1), which are derived from the Hartree–Fock techniques with periodic boundary conditions employing the CRYSTAL code [30], are used as components of the cost function. Further details of the latter calculations are given in the Appendix.

Morse potentials are used for the B–O interactions. Indeed when a Buckingham potential was used for this interaction no acceptable solution was obtained. As noted, Morse functions

model covalent bonding and as such they can compensate for some part of the lattice energy that is lost on reducing the effective charges, so a 90% ionicity model is used instead of the formal charge in the first three potentials (A1 to A3). Buckingham potentials are used for the O–O and B–B interactions. Potential A1 includes pair, three-body plus four-body terms (discussed below); potential A2 includes pair and three-body terms and potential A3 includes only pair-potential terms. In potential A4 and potential A5 charges are reduced to 50% and 40% ionicity.

Table 5. Static lattice simulation of the structure and properties of B_2O_3-I using fitted potentials (A1–A5). The experiment data [24] are given in brackets.

	Potential sets for static lattice simulation					
	A1	A2	A3	A4	A5	
(i) Calculated lattice energies in experimental (E1) and energy-minimized (E2) structures (eV/B_2O_3)						
E1	−182.47	−183.95	−181.11	−52.99	−34.81	
E2	−182.76	−184.81	−181.70	−53.05	−34.90	
(ii) Energy-minimized structure (percentage error with respect to experimental value); unit-cell volume (v), lattice constants (a, b, c) (%)						
v	+ 1.89	−3 60	+ 2.05	−2.92	−5.48	
a	+ 1.49	+ 0.79	+ 2.54	+ 0.19	+ 0.04	
b	+ 1.49	+ 0.79	+ 2.54	+ 0.19	+ 0.04	
c	−1.09	−5.09	−2.94	−3.29	−5.55	
Bond length (Å)						
B1–O1	1.386	1.375	1.372	1.405	1.393	(1.404)
B1–O2	1.358	1.384	1.374	1.357	1.371	(1.366)
B1–O3	1.366	1.384	1.373	1.374	1.381	(1.337)
B2–O1	1.358	1.385	1.374	1.356	1.371	(1.336)
B2–O2	1.386	1.375	1.372	1.404	1.392	(1.400)
B2–O3	1.366	1.384	1.373	1.375	1.382	(1.384)
Bond angle (deg)						
O1–B1–O2	120.3	118.6	119.1	119.3	118.7	(119.0)
O1–B1–O3	117.7	121.4	120.7	115.4	117.6	(114.7)
O2–B1–O3	122.0	119.9	120.2	125.2	123.6	(126.1)
O1–B2–O2	120.3	118.5	119.1	119.3	118.7	(121.5)
B1–O1–B2	134.7	134.6	140.1	130.4	131.1	(130.5)
B1–O2–B2	134.7	134.6	140.1	130.4	131.2	(128.3)
(iii) Properties for energy-minimized structures						
Elastic constant (GPa)						
$E(1, 1)$	473.9	642.7	488.5	176.5	116.7	
$E(1, 2)$	122.8	157.9	96.4	52.3	32.4	
Bulk modulus (GPa)						
	239.8	319.5	227.1	93.7	60.5	
Static dielectric constant (experiment: 3.0–3.5)[a]						
$\varepsilon_0(1, 1)$	1.64	2.08	2.17	1.80	1.84	
$\varepsilon_0(2, 2)$	1.64	2.08	2.17	1.80	1.84	
$\varepsilon_0(3, 3)$	1.68	4.05	2.77	2.41	2.57	

[a] From [27].

The four-body term, included in potential A3 is a torsional term applied around the O–B–O–O bond angle in the BO_3 triangle and is often taken to be of the form:

$$V = K_4(1 - \cos(2\phi)) \tag{21}$$

where K_4 is a force constant and ϕ is the torsion angle. This term is added to retain planarity of the BO_3 triangle, as shown in figure 3.

The fitted potential parameters are shown in table 4 and the resulting static lattice simulations for both B_2O_3-I and B_2O_3-II are given in tables 5 and 6 respectively.

Table 6. Static lattice simulation of the structure and properties of B_2O_3-II using fitted potentials (A1–A5). Experiment data [25] in bracket.

	Potential sets					
	A1	A2	A3	A4	A5	
(i) Calculated lattice energies in experimental (E1) and energy-minimized (E2) structures (eV/B_2O_3)						
E1	−183.74	−183.89	−179.54	−54.08	−35.70	
E2	−184.12	−184.20	−180.08	−54.29	−35.77	
(ii) Energy-minimized structure (percentage error with respect to experimental value); unit-cell volume (v), lattice constants (a, b, c) (%)						
v	+ 0.52	+ 4.12	+ 5.15	+ 3.83	+ 0.56	
a	+ 0.24	+ 0.94	+ 2.11	+ 0.48	−0.38	
b	+ 0.24	+ 0.94	+ 2.11	+ 0.48	−0.38	
c	−0.33	+ 2.03	+ 1.12	+ 1.82	+ 0.96	
Bond length (Å)						
B1–O1	1.429	1.398	1.445	1.393	1.406	(1.373)
B1–O2	1.450	1.492	1.509	1.439	1.462	(1.506)
B1–O2′	1.471	1.540	1.510	1.470	1.497	(1.508)
B1–O2″	1.532	1.555	1.521	1.672	1.553	(1.512)
Bond angle (deg)						
O1–B1–O2	107.1	110.3	111.0	104.1	106.8	(110.2)
O1–B1–O2′	113.6	114.4	110.8	117.0	115.2	(115.8)
O1–B1–O2″	111.3	111.7	111.8	112.5	111.8	(113.1)
O2–B1–O2′	109.3	110.6	108.1	109.3	110.4	(107.4)
B1–O1–B1	138.6	138.7	142.0	131.5	134.7	(138.6)
B1–O2–B1	119.3	118.5	117.7	119.3	118.7	(118.7)
(iii) Properties for energy-minimized structures						
Elastic constant (GPa)						
$E(1, 1)$	1429.6	1339.7	1179.3	257.0	265.7	
$E(1, 2)$	167.2	217.2	89.9	−26.9	45.3	
Bulk modulus (GPa)						
	588.0	591.4	453.0	67.8	118.7	
Static dielectric constant (experiment: 3.0–3.5)[a]						
$\varepsilon_0(1, 1)$	2.33	2.24	3.09	2.02	2.19	
$\varepsilon_0(2, 2)$	2.45	3.45	4.58	1.83	3.35	
$\varepsilon_0(3, 3)$	2.43	3.16	5.78	1.82	2.40	

[a] From [27].

The first clear result of the fitting exercise is that on comparing potentials A1, A2 and A3, we find that the pair-potential model (A3) is very poor in describing the B–O–B bond angles and the cell volume (and hence density), as discussed in section 4. It is interesting to note that the fitted O–B–O force constant is zero both for potential A1 and A2. This may mean that the effects of the O–B–O interactions can be mimicked by the O–O interactions, while the B–O–B interactions cannot easily be replaced with the B–B interactions. It is also of considerable interest that the potentials which are fitted only using the data of B_2O_3-I can reproduce the structure of B_2O_3-II well.

Turning now to the question of the atomic charges, the experimental structure is relatively insensitive to their value if we allow the short-range potentials to be refitted; in contrast the elastic constants and the bulk modulus are strongly dependent upon the values assigned to these charges. Generally speaking, the more ionic models have the larger bulk moduli. When the bulk modulus (30–50 GPa for B_2O_3-I and 100–130 GPa for

B_2O_3-II) calculated in the companion *ab initio* study of B_2O_3 [2, 3] are taken into account, an effective charge of 40% or less of the formal value may be appropriate. Ionicities of this magnitude also agree with the Mulliken charge ($qB \simeq +1.2$) calculated by Takada [2].

We also note that for the rigid ion model, the calculated static dielectric constants are smaller than the experimental values (3.0–3.5) [27] as expected. Use of the shell model may overcome such problems.

Table 7. Fitted potentials (B1, C1, C2) based on both crystal structures and *ab initio* data.

	Potential sets		
Parameters	B1	C1	C2
Charge			
q(B)	+1.2	+1.2	+0.9
q(O)	−0.8	−0.8	−0.6
Morse potential for B–O for twofold oxygen atom O2			
D (eV)	2.322	1.84	1.79
β (Å^{-1})	2.5	2.7	2.7
ρ_0 (Å)	1.35	1.35	1.35
for threefold oxygen atom O3			
D (eV)	2.322	0 98	0.96
β (Å^{-1})	2.5	2.7	2.7
ρ_0 (Å)	1.35	1.475	1.475
Buckingham potential for O–O			
A (eV) for O_2–O_2	2231.5	1990.8	485.8
A (eV) for O_2–O_3	2231.5	1650.9	422.9
A (eV) for O_3–O_3	2231.5	692.3	193.4
ρ (Å)	0.30	0.30	0.35
C (eV Å^6)	0.0	0.0	0.0
Buckingham potential for B–B			
A (eV)	0	323.1	0.0
ρ(Å)	0.30	0.30	0.35
C (eV Å^6)	0.0	0.0	0.0
Three-body term for O–B–O ($\theta_0 = 120°$ for threefold; $\theta_0 = 109.47°$ for fourfold) for threefold boron atom			
k (eV rad^{-2})	2.0	0	3.24
for fourfold boron atom			
k (eV rad^{-2})	2.0	1.66	1.94
Three-body term for B–O–B ($\theta_0 = 120°$) for twofold oxygen atom			
k (eV rad^{-2})	5.58	6.38	4.60
for threefold oxygen atom			
k (eV rad^{-2})	5.58	4.22	4.53
four-body term for O–B–O–O			
k (eV rad^{-2})	0.02	—	—

6.1.2. Fitting to both B_2O_3-I and B_2O_3-II structures. Next, in order to reproduce better the structures of both B_2O_3-I and B_2O_3-II, simultaneous fitting is performed. For B_2O_3-I, twelve structural configurations (lattice constants are varied) and eleven *ab initio* data (see table A1) are used for the structural stability conditions and as components of the cost function respectively; while for B_2O_3-II, we use twelve structural configurations and eleven

ab initio data. The fitted potential (potential B1) and the resulting static lattice simulations are shown in tables 7–9.

Table 8. Static lattice simulation of the structure and properties of B_2O_3-I using fitted potentials (B1, C1, C2). Experimental data [24] are given in brackets.

	Potential sets			
	B1	C1	C2	
(i) Calculated lattice energies in experimental (E1) and energy-minimized (E2) structures (eV/B_2O_3)				
E1	−44.74	−42.05	−27.16	
E2	−44.83	−42.11	−27.24	
(ii) Energy-minimized structure (percentage error with respect to experimental value); unit-cell volume (v), lattice constants (a, b, c) (%)				
v	+ 0.30	+ 1.87	+ 1.32	
a	+ 0.89	+ 0.87	+ 0.83	
b	+ 0.89	+ 0.87	+ 0.83	
c	−1.47	+ 0.12	−0.34	
Bond length (Å)				
B1–O1	1.396	1.409	1.398	(1.404)
B1–O2	1.358	1.346	1.367	(1.366)
B1–O3	1.365	1.362	1.364	(1.337)
B2–O1	1.358	1.346	1.367	(1.336)
B2–O2	1.396	1.409	1.398	(1.400)
B2–O3	1.365	1.362	1.364	(1.384)
Bond angle (deg)				
O1–B1–O2	120.3	120.1	120.4	(119.0)
O1–B1–O3	116.6	115.3	116.1	(114.7)
O2–B1–O3	122.7	124.0	121.7	(126.1)
O1–B2–O2	120.3	120.1	120.4	(121.5)
B1–O1–B2	131.9	131.4	130.7	(130.5)
B1–O2–B2	131.9	131.4	130.7	(128.3)
(iii) Properties for energy-minimized structures				
Elastic constant (GPa)				
$E(1, 1)$	223.4	191.6	138.6	
$E(1, 2)$	58.9	52.4	38.5	
Bulk modulus (GPa)				
	113.8	98.8	71.9	
Static dielectric constant (experiment: 3.0–3.5)[a]				
$\varepsilon_0(1, 1)$	1.44	1.60	1.40	
$\varepsilon_0(2, 2)$	1.44	1.60	1.40	
$\varepsilon_0(3, 3)$	2.13	2.38	2.59	

[a] From [27].

We find that potential B1 can reproduce both crystal structures very well. The simultaneous fitting reproduces both structures equally well. However, two problems still remain. The first is that the difference in the B–O bond lengths in the B_2O_3-II structure is not well reproduced. As discussed by Takada [2], the coordination numbers around O1 and O2 are two and three which is thought to be the main reason for differences in the B–O bond lengths. The second problem is that the lattice energy of B_2O_3-II is sometimes lower or almost the same as that of B_2O_3-I. This tendency becomes stronger as the ionic charges are reduced and is clearly a substantial problem.

In order to overcome these difficulties, we have further developed our approach. We recall from the companion *ab initio* study [2] of B_2O_3 that the B–O bond strength changes according to its coordination number. Moreover, in the case of B_2O_3, the coordination

Table 9. Static lattice simulation of the structure and properties of B_2O_3-*II* using fitted potentials (B1, C1, C2). Experimental data [25] are given in brackets.

	Potential sets			
	B1	C1	C2	
(i) Calculated lattice energies in experimental (E1) and energy-minimized (E2) structures (eV/B_2O_3)				
E1	−44.50	−40.70	−25.77	
E2	−44.73	−40.84	−25.84	
(ii) Energy-minimized structure (percentage error with respect to experimental value); unit-cell volume (v), lattice constants (a, b, c) (%)				
v	+ 1.52	−2.53	−1.96	
a	+ 0.09	−0.27	−0.79	
b	+ 0.09	−0.27	−0.79	
c	+ 0.75	−0.49	+ 0.42	
Bond length (Å)				
B1–O1	1.419	1.346	1.367	(1.373)
B1–O2	1.449	1.476	1.489	(1.506)
B1–O2′	1.469	1.502	1.501	(1.508)
B1–O2″	1.597	1.564	1.543	(1.512)
Bond angle (deg)				
O1–B1–O2	105.8	110.6	109.5	(110.2)
O1–B1–O2′	113.5	117.9	116.1	(115.8)
O1–B1–O2″	112.3	115.2	114.3	(113.1)
O2–B1–O2′	109.3	107.5	108.3	(107.4)
B1–O1–B1	133.5	134.1	133.2	(138.6)
B1–O2–B1	118.8	120.0	119.7	(118.7)
(iii) Properties for energy-minimized structures				
Elastic constant (GPa)				
$E(1, 1)$	531 4	577.4	403.2	
$E(1, 2)$	−3.0	83.2	65.7	
Bulk modulus (GPa)				
	175.1	248.0	178.2	
Static dielectric constant (experiment: 3.0–3.5)[a]				
$\varepsilon_0(1, 1)$	1.67	1.59	1.32	
$\varepsilon_0(2, 2)$	1.56	1.65	1.34	
$\varepsilon_0(3, 3)$	1.57	1.68	1.40	

[a] From [27].

number around the oxygen atoms seems to be especially important. Therefore, different Morse and Buckingham potentials are assigned for twofold- and threefold-coordinated oxygen. Next, in order to keep the energy of B_2O_3-I lower than that of B_2O_3-II, one inequality condition:

$$E_{B_2O_3-I} < E_{B_2O_3-II} \tag{22}$$

is added during the fitting.

The fitted potentials (C1 and C2) and the resulting static lattice simulations are again given in tables 7–9. Potential C1 is fitted with charges corresponding to 40% ionicity, while that for C2 was 30%. Both potentials reproduce not only the lattice parameters but also the bond lengths and bond angles in the two crystals, while keeping the energy of B_2O_3-I lower than that of B_2O_3-II.

6.1.3. LP fitting potentials based on periodic HF energy surfaces: summary. We have succeeded in deriving several sets of potentials which can reproduce both crystal structures

of B_2O_3. In particular, we find that a partial charge model with a B–O Morse potential and a B–O–B bond-bending, three-body term can reproduce both crystal structures accurately. The comparison of the lattice energies of the two structures suggests that different short-range potentials must be defined to reproduce the order of their energies, and the potential sets (C1 and C2) in which parameters depend on the coordination number around the oxygen atoms have consequently been developed. These potentials can reproduce not only the structures but also the order of the lattice energies of the two phases. They will be applied to MD simulations of vitreous B_2O_3 in subsequent papers.

6.2. *Potentials derived from molecular clusters and crystals*

6.2.1. Potentials derived only from molecular clusters. Can potential energy surfaces based on molecular systems enjoy similar success to those based on periodic structures?

For the SiO_2 system, several sets of interatomic potentials derived from *ab initio* calculations on related molecular clusters have been applied to crystalline and vitreous states. In the B_2O_3 system, Gupta and Tossell [31, 32], Gibbs *et al* [33] and Zhang *et al* [34] showed that molecular clusters mimic the geometry of polyanions in borate minerals. A detailed study of molecular energy surfaces is therefore reported in this section.

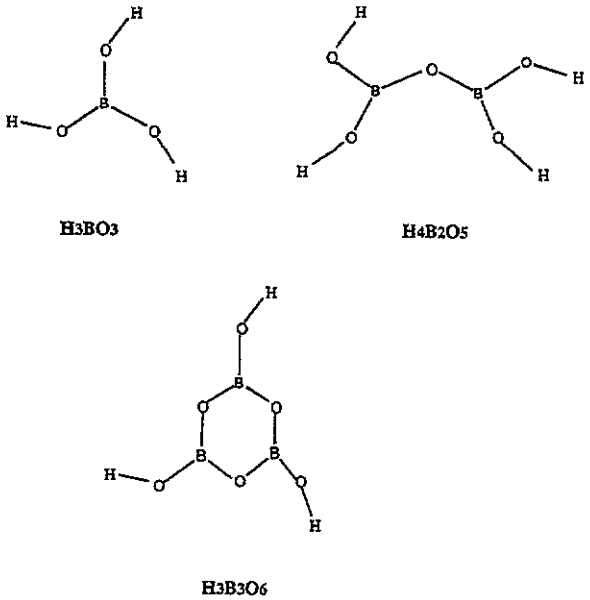

Figure 4. Molecular clusters used for deriving potentials.

To this end we have therefore calculated several potential energy surfaces for molecular clusters, by performing *ab initio* calculations on the monomer HBO_3, the dimer $H_4B_2O_5$ and the trimer $H_3B_3O_6$ using a 6-31G* basis set with the GAUSSIAN-90 program [35]. The schematic diagrams of the three structures are shown in figure 4. For HBO_3, we optimized with C_1 symmetry; after optimization, the B–O bond lengths (whose optimized value is 1.374 Å) are varied from 1.0 Å to 2.0 Å and the O–B–O bond angles are varied from 105° to 135°. For $H_4B_2O_5$, the structure is optimized with C_2 symmetry; following the optimization, the B–O–B bond angle (the optimized value of which is 134.5°) is varied from 120° to 150°. The structure of $H_3B_3O_6$ is optimized subject to C_{3h} symmetry and the

O–B–O and the B–O–B angles remain fixed at 120°. The optimized B–O bond length is 1.384 Å for in-ring bonds and 1.358 Å for out-of-ring bonds.

There are several assumptions made in deriving the resulting potentials. In order to keep charge neutrality, the charge of the hydrogen atom (q_H) is varied, with the charges of boron atom (q_B) and oxygen (q_O) being changed in order to satisfy the following conditions:

$$q_B = 3q_H \qquad q_O = -2q_H.$$

For the hydrogen atoms we only allow the point charge (q_H) to vary. The interactions between the oxygen and hydrogen atoms in the OH group are assumed to be unchanged, because the O–H bond lengths remain fixed in the *ab initio* calculations.

We employ a general least-square fitting procedure of interatomic potential parameters to the *ab initio* energy surfaces, varying the charge q_H. We used partial charge models with Buckingham potentials for the B–O and O–O interactions and bond-bending, three-body terms for the O–B–O and B–O–B interactions. A total of eight parameters (A, ρ, and C parameters for the B–O and O–O interactions; bond-bending force constants for the O–B–O and B–O–B interactions), but not the charges were fitted. In order to check the influences of the range of *ab initio* data employed in the fitting procedures, two potentials are fitted. Potentials D1 and D2 are fitted using respectively the 'long-range' B–O data, i.e. (1.0 Å < R(B–O) < 2.0 Å) and the 'short-range' B–O data, i.e. (1.15 Å < R(B–O) < 1.55 Å). The 'short-range' B–O data are of course present in the 'long-range' B–O data. The fitted potentials are given in table 10.

Table 10. Fitted potentials (D1, D2) obtained using *ab initio* data on molecular clusters.

Parameter	Potential D1	Potential D2
Charge		
q(B)	+1.11	+1.11
q(O)	−0.74	−0.74
Buckingham potential for B–O		
A (eV)	1843.0	592.4
ρ (Å)	0.169	0.192
C (eV Å^6)	0	0
Buckingham potential for O–O		
A (eV)	1919.8	8207.0
ρ (Å)	0.284	0.235
C (eV Å^6)	0	0
Three-body terms for O–B–O (θ_0 = 120°) and B–O–B (θ_0 = 120°)		
k(O–B–O)	0.0004	1.675
k(B–O–B)	1.625	1.251

When used in modelling the B_2O_3-I crystal, both potentials D1 or D2 result in an expansion of the cell volume by 35% or 17%. Several other attempts were made to fit the data (for example, using a Morse potential or with different charges), but none of them could reproduce the B_2O_3 structure well. It appears that the effects of the crystalline environments are not simply expressed by the addition of the electrostatic Madelung potential; and the results may suggest moreover that the short-range terms must be varied in line with the change of charge distribution due to the crystalline environments. A more detailed discussion is given in the following section.

Table 11. Input data and conditions used for LP fitting. For the monomer, dimer and trimer, $R_{(B-O)}$ and $\theta_{(O-B-O)}$, $\theta_{(B-O_{br}-B)}$, $R_{(B-O_{br})}$ and $R_{(B-O_{nbr})}$ varied; for crystals, a, b, c, α, β, γ varied. R, θ and a, b, c, α, β, γ represent bond lengths, angles and lattice constants. O_{br} and O_{nbr} represent non-bridging and bridging oxygen atoms. (Note that the energies are calculated using the standard Hartree–Fock procedures described in the text and are available from the authors on request.)

	Component of cost function Derived from *ab initio* data	Structural stability condition Derived from structural data
Monomer HBO_3	(10 structural configurations used for fitting)	(2 structural configurations used for fitting)
$E = E(R_{(B-O)}, \theta_{(O-B-O)})$	$E(1.374, 120)$, $E(1.3, 120)$,	$E(1.384, 120) > E(1.374, 120)$
	$E(1.35, 120)$, $E(1.40, 120)$,	$E(1.364, 120) > E(1.374, 120)$
Energy-minimized value	$E(1.45, 120)$, $E(1.50, 120)$,	
$R_{(B-O)} = 1.374$	$E(1.374, 110)$, $E(1.374, 115)$,	
$\theta_{(O-B-O)} = 120.$	$E(1.374, 125)$, $E(1.374, 130)$	
Dimer $H_4B_2O_5$	(7 structural configurations used for fitting)	(2 structural configurations used for fitting)
$E = E(\theta_{(B-O_{br}-B)})$	$E(134.5)$, $E(120)$,	$E(139.5) > E(134.5)$
Energy-minimized value	$E(125)$, $E(130)$,	$E(129.5) > E(134.5)$
$R_{(B-O_{br})} = 1.365$	$E(140)$, $E(145)$,	
$R_{(B-O_{nbr})} = 1.3557$	$E(150)$	
$\theta_{(O-B-O)} = 134.5$		
Trimer $H_3B_3O_6$	(no data used)	(4 structural configurations used for fitting)
$E = E(R_{(B-O_{br})}, R_{(B-O_{nbr})})$		$E(1.374, 1.358) > E(1.384, 1.358)$
Energy-minimized value		$E(1.364, 1.358) > E(1.384, 1.358)$
$R_{(B-O_{br})} = 1.384$		$E(1.384, 1.368) > E(1.384, 1.358)$
$R_{(B--O_{nbr})} = 1.358$		$E(1.384, 1.348) > E(1.384, 1.358)$
B_2O_3-I crystal	(9 structural configurations used for fitting)	(12 structural configurations used for fitting)
$E = E(a, b, c, \alpha, \beta, \gamma)$	E(exp),	$E(a: +1\%\text{or} -1\%) > E$(exp)
	$E(a, b, c: +4\%)$, $E(a, b, c: +2\%)$,	$E(b: +1\%\text{or} -1\%) > E$(exp)
	$E(a, b, c: -4\%)$, $E(a, b, c: -2\%)$,	$E(c: +1\%\text{or} -1\%) > E$(exp)
	$E(c: +3\%)$, $E(c: -2\%)$,	$E(\alpha: +2.5°\text{or} -2.5)° > E$(exp)
Exp = experimentally observed structure	$E(a: +2\%)$, $E(a: -1\%)$	$E(\beta: +2.5°\text{or} -2.5)° > E$(exp)
		$E(\gamma: +2.5°\text{or} -2.5)° > E$(exp)
B_2O_3-II crystal	(no data used)	(12 structural configurations used for fitting)
$E = E(a, b, c, \alpha, \beta, \gamma)$		$E(a: +1\%\text{or} -1\%) > E$(exp)
		$E(b: +1\%\text{or} -1\%) > E$(exp)
		$E(c: +1\%\text{or} -1\%) > E$(exp)
		$E(\alpha: +2.5°\text{or} -2.5)° > E$(exp)
Exp = experimentally observed structure		$E(\beta: +2.5°\text{or} -2.5)° > E$(exp)
		$E(\gamma: +2.5°\text{or} -2.5)° > E$(exp)

6.2.2. Potentials derived from both crystals and molecular clusters. In the previous section, the simple application of the potentials derived from the *ab initio* data on the molecular clusters failed to reproduce the B_2O_3-I structure. Is there any common potential transferable for both crystal structures and molecular clusters?

To investigate this problem, several simultaneous LP fitting calculations were performed using both the crystal structural and the molecular cluster data. GAUSSIAN-derived and CRYSTAL-derived *ab initio* data were used for molecular clusters and crystals respectively.

Table 12. Summary of conditions used in LP fitting for potentials E1 to E7. @ indicates data used during LP fitting.

	Fitted potential sets						
Parameters	E1	E2	E3	E4	E5	E6	E7
Charge							
q(B)	+1.2	+1.2	+1.2	+0.6	+0.6	+0.6	+0.6
q(O)	−0.8	−0.8	−0.8	−0.4	−0.4	−0.4	−0.4
Monomer							
ab initio data	@		@	@		@	@
stability condition			@			@	@
Dimer							
ab initio data	@		@	@		@	@
stability condition			@			@	@
Trimer							
Stability condition			@			@	@
B_2O_3-I crystal							
ab initio data		@			@		@
Stability condition	@	@		@	@		@
B_2O_3-II crystal							
Stability condition	@	@		@	@		

Table 13. *LP fitted potentials obtained using molecular data and crystal data (E1–E7).*

	Fitted potential sets						
Parameter	E1	E2	E3	E4	E5	E6	E7
Charge							
q(B)	+1.2	+1.2	+1.2	+0.6	+0.6	+0.6	+0.6
q(O)	−0.8	−0.8	−0.8	−0.4	−0.4	−0.4	−0.4
Morse potential for B–O							
D (eV)	2.48	2.53	4.05	2.65	3.90	4.28	4.09
β (Å^{-1})	2.7	2.7	2.7	2.9	2.7	2.7	2.8
ρ_0 (Å)	1.35	1.35	1.30	1.28	1.28	1.28	1.28
Buckingham potential for O–O							
A (eV)	2250	2286	1679	1632	2245	2371	2447
ρ (Å)	0.30	0.30	0.30	0.30	0.30	0.30	0.30
C (eV Å^6)	0	0	0	0	0.1	37.1	42.0
Buckingham potential for B–B							
A (eV)	0	0	440.8	0	0	1348	1290
ρ (Å)	0.30	0.30	0.30	0.30	0.30	0.30	0.30
C (eV Å^6)	0	0	0	0	0	0	0
Three-body term for O–B–O (k_3, $\theta_0 = 120°$ for threefold; k_4, $\theta_0 = 109.47°$ for fourfold)							
k_3 (eV rad^{-2})	0	0	0.93	1.09	0	0.08	0.01
k_4 (eV rad^{-2})	5.00	1.78	—	7.47	17.79	—	1.04
Three-body term for B–O–B ($\theta_0 = 120°$)							
k (eV rad^{-2})	1.37	4.47	0.50	0.14	0.02	0.88	1.04

LP fitting is very suitable for this sort of study, because the conditions for molecular clusters and crystals are dealt with independently and equally. The input data and conditions used

for the LP fitting are shown in tables 11 and 12. A total of seven fitting calculations were performed which differ in the data that were used; the fitted potentials and the resulting static lattice simulations are shown in tables 13 and 14.

Table 14. Static lattice simulation using the fitted potentials (E1–E7). # indicates a calculated value which deviates considerably from experiment. * indicates an averaged bond angle. ## indicates a result where one angle is much larger and the other is much smaller than that of experiment.

Parameter	Potential sets for static lattice simulation							⟨Experimental data⟩
	E1	E2	E3	E4	E5	E6	E7	
Monomer *bond length R (Å)*								
R(B–O)	1.374	1.464#	1.374	1.384	1.394	1.374	1.374	⟨1.374⟩
Dimer *bond length R (Å) and bond angle θ (deg)*								
$R_{\langle B-O_{br}\rangle}$	1.455#	1.455#	1.365	1.395	1.385	1.365	1.365	⟨1.365⟩
$\theta_{\langle B-O_{br}-B\rangle}$	131.5	127.5	132.5	132.5	144.5#	132.5	133.5	⟨134.5⟩
Trimer *bond lengths* $R_{\langle B-O_{br}\rangle}$ *and* $R_{\langle B-O_{nbr}\rangle}$								
$R_{\langle B-O_{br}\rangle}$	1.459#	1.455#	1.374	1.384	1.384	1.394	1.394	⟨1.384⟩
$R_{\langle B--O_{nbr}\rangle}$	1.458#	1.458#	1.368	1.388	1.398	1.368	1.368	⟨1.358⟩
B_2O_3-I crystal *lattice energy (eV/B_2O_3), relative cell volume to experimental value (%), bond angle* $\theta_{\langle B-O-B\rangle}$								
Energy	−46.21	−46.11	−57.69	−20.38	−26.60	−29.76	−28.39	
Cell volume	+9.8#	+0.9	−25.8#	+11.0#	−5.29	−4.46	+0.93	
$\theta_{\langle B-O-B\rangle}$	140.1#	132.4	126.7	138.5#	##	136.5#	138.5#	⟨130.0*⟩
B_2O_3-II crystal *lattice energy (eV/B_2O_3), relative cell volume to experimental value (%)*								
Energy	−46.31	−46.16	−59.87	−20.14	−26.48	−30.44	−28.64	
Cell volume	+2.1	+0.4	−15.1#	−1.55	+0.50	−2.33	−1.27	

Several features of the calculated results deserve attention. First we note that before investigating the models based on 40% and 20% ionicity (potentials E1–E7), several other values for the ionic charges were tested. In general, the models with higher ionicity (>30%) are good at reproducing the crystal structures, while the lower ionicity models (<20%) reproduce the molecular structures well. 40% ionicity ($q_B = +1.2$, $q_O = -0.8$) is close to the Mulliken charge ($q_B = +1.1$) in B_2O_3-I calculated by the CRYSTAL codes (STO3-21G basis set), and 20% ionicity ($q_B = +0.6$, $q_O = -0.4$) is close to that ($q_B = +0.65$) in HBO_3 calculated by the GAUSSIAN-90 code (MP2/6-311G**). The aim of the present fitting procedure is to explore the possibility of a common potential for both crystals and molecules; so a common charge value is used in the LP fitting, although the crystal is clearly more ionic than the molecules.

We found, not surprisingly in view of the above comments, that when all the conditions are used at the same time in the LP fitting, no feasible solution existed. Therefore, several combinations of conditions are used in the LP fitting.

Potentials E3 and E6 refer to the case where only molecular *ab initio* data (obtained from the GAUSSIAN calculations) and the stability conditions of the molecules are used without any data relating to the crystals. It is interesting to note that the D parameter in the B–O Morse potential is larger than those of the other cases, which leads to the smaller cell volume in B_2O_3-I. We also find that the experimental B–O bond lengths in the crystalline states are almost the same as those calculated from the *ab initio* simulations for the molecules (see tables 11 and 15). Thus in the molecules, although there are no crystal effects (due to long-range electrostatic forces), the bond lengths are close to those in the crystalline state, but the B–O covalent bonding as represented by the Morse term becomes

Table 15. B–O bond distances in borate minerals.

Compound	B–O (Å) Triangular BO_3	B–O (Å) Tetrahedral BO_4	Reference
Boron trioxide			
B_2O_3-I	1.337, 1.366, 1.404		[24]
	1.336, 1.384, 1.401		
B_2O_3-II		1.373, 1.506, 1.507, 1.512	[25]
Orthoboric acid			
$B(OH)_3$	1.356, 1.365, 1.365		[36, 37]
	1.353, 1.359, 1.365		
Metaboric acid			
HBO_2-I			[38]
	1.345, 1.371, 1.386		
	1.356, 1.366, 1.378		
		1.433, 1.451, 1.452, 1.553	
HBO_2-II			[39]
		1.436, 1.465, 1.482, 1.505	
HBO_2-III			[40, 41]
	1.373, 1.377,		
	1.391, 1.353,		
	1.372, 1.372 (in-ring)		
	1.351, 1 367, 1.347 (out-of-ring)		

stronger than in the crystals.

Potentials E1 and E4 refer to the case where the *ab initio* data *on the molecules* (GAUSSIAN-derived data) are used as components of the cost function, while the stability conditions *of the crystals* are imposed. The fitted results give a smaller D value in the B–O Morse potential and a larger force constant (K) of the B–O–B interactions, compared with those of potentials E3 and E6. The smaller D value suggests that in the crystalline states the effects of the crystal field replace a component of the B–O attractive terms described in terms of covalence in the molecular species. A possible reason for the large K value may be that in the crystal the larger effective charges result in an increased repulsion between the B atoms, which is not modelled directly owing to the use of a common set of charges for the molecules and crystals; this error in the Coulomb term is compensated by the increase in the bond-bending interaction.

Potentials E2 and E5 show the case where only *ab initio* data (CRYSTAL-derived data) and the structural stability conditions of the crystals are used. The use of too many conditions for LP fitting occasionally gave no feasible solution. Therefore, the number of conditions used for LP fitting was reduced, compared with that in our earlier potentials (B1, C1 and C2). As for potential E2, both crystal structures are reproduced very well, in contrast to the potential based on molecular calculations which result in long B–O bond lengths. Unlike the case of potentials E3 and E6, the D parameter in the B–O Morse potential has a small value corresponding to the crystalline state. We note that potential E5 fails to reproduce the structure of B_2O_3-I; the relaxed structure, using this potential, has fourfold coordination around the boron atoms. In general, the smaller the value of the charge used, the more difficult becomes the simultaneous fitting of B_2O_3-I and B_2O_3-II and low-charge models cannot reproduce both structures with a single set of parameters. A likely explanation of the latter feature is that low-charge models cannot compensate the difference between the Madelung energies of the two polymorphs.

Potential E7 was derived using both molecular and crystal *ab initio* data (i.e. from both GAUSSIAN and CRYSTAL calculations) for B_2O_3-I. There is no feasible solution for 40% or higher charge models, or in the case where the data for B_2O_3-II is added. However, this potential reproduces the B–O bond lengths for the three molecules and the cell volumes in both crystals reasonably with the same set of parameters, although the B–O–B bond angle in B_2O_3-I shows appreciable error. It suggests that it is difficult to reproduce both molecular and crystalline structures precisely with a common potential, but that the 20% charge model can reproduce them both to some extent.

There are two problems remaining in applying these potentials to MD simulations. One is the large C value in the O–O interactions fitted in the 20% ionicity model. It generates too large an attractive force when the O–O distance becomes short. The other is the energy difference between B_2O_3-I and B_2O_3-II. In the case of potentials E1, E2, E3, E6 and E7, the energy of B_2O_3-II is lower than that of B_2O_3-I. During the LP fitting, one inequality condition $E_{B_2O_3-I} < E_{B_2O_3-II}$ can be added, but it is very difficult to find an acceptable solution for the smaller charge models (20% or less) which still reproduces both structures. We proceed to MD simulations using these and better potentials in our subsequent study.

It appears therefore to be difficult to find transferable potential models that reproduce the two crystal structures and the three molecular structures with a common set of parameters. Even the best model often fails to reproduce the order of the lattice energies. When compared with the 'molecular' potentials, the 'crystalline' potentials result in higher charge models, with the B–O attractive terms being weaker and the force constant of the B–O–B interactions being larger.

Finally, it is interesting to note that although the bond lengths and bond angles are very similar for the molecular and the crystalline states, the potentials parameters are different reflecting the differing degrees of ionicity in molecules and crystals.

6.3. Potentials for B_2O_3: summary

We have found that it is essential to employ a partial charge model with a B–O Morse potential and a B–O–B bond-bending, three-body term in order to reproduce both crystal structures accurately. Moreover, to reproduce the order of energies in different phases, new potentials (C1 and C2), which depend on the coordination number around the oxygen atoms have been developed.

When we compare the 'molecular' potentials (e.g. E3 or E6) with the 'crystalline' potentials (e.g. A, B, C, E2 or E5), we have found that it is possible to fit molecular or crystal data separately, but that the potentials are not transferable. When we attempt to derive common potentials (E1, E4 or E7), by fitting both to molecular and crystalline data simultaneously, these do not reproduce both the crystal structures and the three molecular structures. These results must cast considerable doubt on the use of calculations on small molecules in modelling the properties of ionic or semi-ionic solids.

We will now use the more successful of our potentials to investigate the stability of various polymorphic structures of B_2O_3.

7. 'Computer synthesis' of new possible polymorphs and possible structural units of vitreous B_2O_3

We now investigate whether it is possible to construct polymorphs based on a variety of boroxol ring structures, our motivation being the importance of the boroxol ring in amorphous B_2O_3, a point to which we return in the next paper. We will report several

computer experiments which were performed in order to explore new structures for B_2O_3. The starting point was to identify those structures among the borate crystals that have boroxol ring content. We have discussed elsewhere [2] that the structure of B_2O_3 considerably differs from the borate structures which have a high content of modifier oxides; and as the content of modifier oxides increases, a three-dimensional type of infinite network changes into an assembly of isolated structural units with non-bridging oxygen atoms. Therefore, it is desirable to start from the borate structure with the least content of modifier oxides. Caesium enneaborate [42] $Cs_2O \cdot 9B_2O_3$ is a good first candidate. This structure has two three-dimensional interlocking, twin networks based on B–O bonds (see figure 5). The topology is such that it is not possible to pass from one network to the other. The network comprises two kinds of basic unit (with a ratio 1:2): a triborate group (containing a six-membered ring, but with one of the boron atoms coordinated tetrahedrally with oxygen atoms) and a boroxol group. As noted above, the vitreous structure of B_2O_3 is claimed to have a high fraction of boroxol rings, and a structure such as that of metaboric acid HBO_2-III [41], which comprises only boroxol rings, with only a small influence due to H_2O, is another good starting structure. Its structure is hydrogen bonded with sheets of trimeric HBO_2 molecules (six-membered rings) loosely stacked to form a mica-like plate crystal in the orthorhombic system [41] as shown in figure 6.

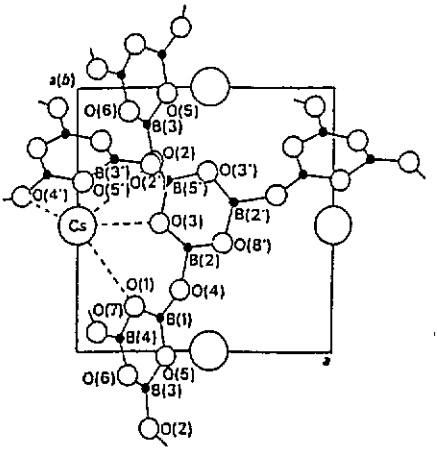

Figure 5. Crystal structures of $Cs_2O \cdot 9B_2O_3$ [42].

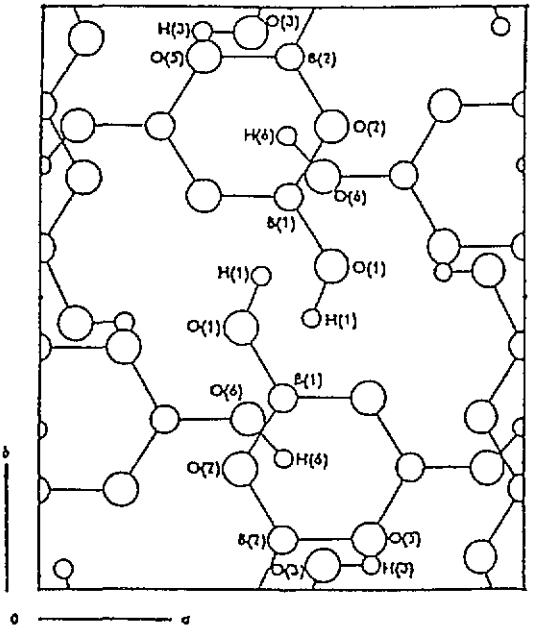

Figure 6. Crystal structure of HBO_2-III [41].

7.1. Construction of new polymorphs from HBO_2-III

It is necessary first to 'dehydrate' HBO_2-III (computationally), for which there are several possible routes. The simplest involves rearrangement of some of the hydrogen bonding between the layers. Two of the three hydroxyl groups, –O(3)H(3) and –O(6)H(6), are almost directly above and below the BO_3 groups of the boron atoms B(1) and B(2), while

the remaining –O(1)H(1) group interacts to a lesser degree with its centre-related counterpart [43] (see figure 6). Therefore firstly, all the O(1) atoms are removed with all the H(1) hydrogen atoms. Next, we extract half of the O(3) and O(6) atoms, and all the H(3) and H(6) atoms. The O(3) or O(6) atoms must be removed alternately in the vertical direction so that the bonding of B(1)–O(6) or B(2)–O(3) can be generated.

After the removal of the hydrogen and oxygen atoms, the remaining O(3) and O(6) atoms are moved to the mid-point between the two neighbouring boron atoms to which we may expect them to bond. Next, static lattice simulations are performed using potential C2, which was shown to be the best potential set for crystalline B_2O_3 in our preceding section. To drive the formation of the new B–O bonds, the B–O Morse D parameter is set initially to be five times its normal value and is restored to the original value after the new bonds are established in the structure.

The resulting completely relaxed structure (B_2O_3-a) has the following features: its unit cell includes six molecules; its lattice parameters are $a = 13.63$ Å, $b = 5.73$ Å, $c = 7.79$ Å, $\alpha = 86.0°$, $\beta = 98.7°$, $\gamma = 99.8°$; and its density is 1.17 g cm^{-3}. It comprises 100% boroxol rings with no independent BO_3 triangles. It is interesting to note three further points. The first is that there is a strong resemblance to the vitreous structure in so far as the average B–O bond length is 1.36 Å and the average B–O–B bond angle of the boroxol rings is 128°. Secondly, however, we find that the density of the new structure is much lower than that of the glass (1.84 g cm^{-3}), in line with previous claims that the 100% boroxol model cannot reproduce the glass density [43, 44]. The third point is that although the original structure is layered, the final structure turns out to be close to the two three-dimensional interlocking type of networks, found in the crystal structure of Cs_2O $9B_2O_3$.

In order to get a higher density as measured experimentally, we made a final change to this structure: half of the B_3O_6 units are replaced with a BO_3 unit. After this change, static lattice simulations were performed using the potential C2 in the same manner as for B_2O_3-a.

The resulting completely relaxed structure of (B_2O_3-b) is as follows: its unit cell includes four molecules; its lattice parameters are $a = 10.22$ Å, $b = 5.71$ Å, $c = 6.13$ Å, $\alpha = 78.2°$, $\beta = 87.3°$, $\gamma = 94.6°$; and its density is 1.33 g cm^{-3}. It comprises 100% boroxol rings with no independent BO_3 triangles. All the B–O bond lengths and bond angles are almost same as B_2O_3-a, while the density increases by 14% compared with that for B_2O_3-a. The results show that the final density is strongly affected by the intermediate-range structure Moreover, it still appears difficult to construct a crystal structure that comprises 100% boroxol rings and has the experimental glass density.

7.2. *Construction of new polymorphs from* $Cs_2O \cdot 9B_2O_3$

The first problem here is again how to extract the Cs_2O from the original crystal structure; and we must check whether reasonable new B–O bonded structures can be generated, after the oxygen atoms have been extracted. One of the obvious routes is to extract half of the O(3) atoms so that the O(3)–O(5') bonding is disconnected and new B(2)–O(3) bonding is generated so that the network is reconnected (see figure 5). After these manipulations, static lattice simulations are performed using potential C2 in the same way as with B_2O_3-a.

The completely relaxed structure (B_2O_3-c) is as follows: its unit cell includes eighteen molecules; its lattice parameters are $a = 7.99$ Å, $b = 10.05$ Å, $c = 16.20$ Å, $\alpha = 94.4°$, $\beta = 90.0°$, $\gamma = 90.0°$; and its density is 1.60 g cm^{-3}, which is only 15% smaller than that of B_2O_3 glass. The ratio of B_3O_6 units to BO_3 units is 2 : 3, i.e. 2/3 of the boron atoms are

in boroxol rings. The basic structure comprises interlocking three-dimensional networks as in the structure of $Cs_2O \cdot 9B_2O_3$, but one BO_3 unit connects two neighbouring networks. In the same network, three BO_3 units are connected in series. One BO_3 is connected with two B_3O_6 units, while the other two units are connected with one B_3O_6 unit, as shown in figure 7. The average B–O bond length is 1.36 Å and the average B–O–B bond angle outside the boroxol rings is 128°.

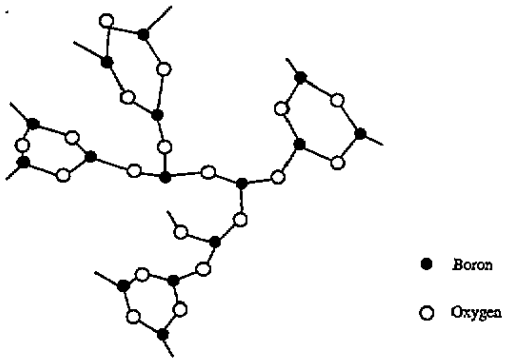

Figure 7. Connection of B_3O_6 units with BO_3 units used in generating B_2O_3-c

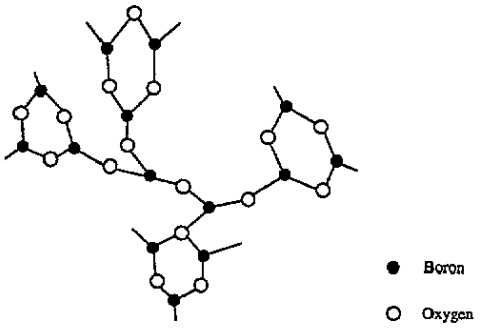

Figure 8. Connection of B_3O_6 units with BO_3 units used in generating B_2O_3-d.

In order to get a density as high as the experimental vitreous density, a final change was made to this structure: two BO_3 units, (B(2), O(3), O(4), O(8')) and (B(2'), O(8), O(4'), O(5')) were replaced with one BO_3 unit simply by topological manipulations, after which static lattice simulations were performed using potential C2 in the same manner as the case of B_2O_3-a. The completely relaxed structure (B_2O_3-d) is as follows: its unit cell includes sixteen molecules; its lattice parameters are $a = 7.94$ Å, $b = 8.58$ Å, $c = 16.55$ Å, $\alpha = 96.1°$, $\beta = 85.0°$, $\gamma = 88.0°$; and its density is 1.72 g cm^{-3}, which is only 6.9% smaller than that of B_2O_3 glass.

The ratio of B_3O_6 units to BO_3 units is 1 : 1, i.e. 75% of the boron atoms are in boroxol rings. The basic structure comprises two interlocking three-dimensional networks without any connection between them, which is the same as in $Cs_2O \cdot 9B_2O_3$. Two BO_3 units are connected in series and each BO_3 unit is connected with two B_3O_6 units. The manner of connection of the BO_3 units is shown in figure 8.

7.3. New polymorphs: discussion and summary

It is interesting to note that all four new structures have almost the same B–O bond lengths and B–O–B bond angles as those observed in B_2O_3-I and vitreous B_2O_3. Although there is no known crystal structure containing boroxol rings, the calculated lattice energies of these four structures are lower than that of B_2O_3-I, and even if they are metastable at finite temperatures, it seems possible that they are candidates for a new polymorph.

On the other hand, for vitreous B_2O_3, it has been claimed that there is no structure model with the experimental density and a high fraction of boron atoms in boroxol rings without layered rings. Crystals constructed in the manner of the layer model proposed by Bell and Carnevale [45] were therefore generated. Six-membered rings, with adjacent sheets overlapping but rotated by $\pi/3$ relative to each other, were hexagonally arranged,

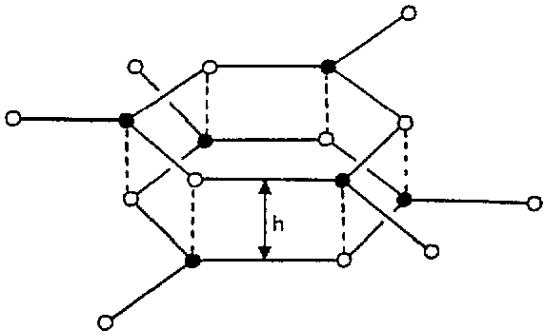

Figure 9. Overlapping B_3O_6 boroxol ring models in adjacent layers of network, relatively rotated by $\pi/3$ rad; 'h' indicates the interlayer distance [45].

as shown in figure 9. The static lattice simulations were performed on these structures, carefully varying the initial interlayer distances. However, the calculated distances between the layers became longer and longer, and a stable structure could not be obtained. Our potential model shows that boric oxide does not favour a layer structure.

Structures B_2O_3-**d** as well as B_2O_3-c could be structural units in vitreous B_2O_3. They have as much as a 75% fraction of boron atoms in boroxol rings and this figure agrees with that estimated for the vitreous material by Jellison *et al* [46] and Johnson *et al* [47]. In addition they not only have reasonable B–O bond lengths and B–O–B bond angles, but they also have a reasonable density, although it is still smaller than that observed for vitreous B_2O_3. Thirdly we note that the structure has a three-dimensional network without layered rings. The most realistic structure for vitreous B_2O_3 is thought to be that in which B_2O_3-c and B_2O_3-d are randomly connected and also some B_3O_6 units are replaced with BO_3 units in order to reproduce the experimental density. The most characteristic feature of such structures is that the three-dimensional networks are interlocking, and two or three BO_3 units are the main connecting parts between B_3O_6 units. The new structures constructed in this paper will be compared with the vitreous structures obtained employing the MD method in the subsequent paper.

7.4. Lattice dynamics simulation

As the final component of this study we report the analysis of the vibrational properties of the new structures. Our investigation is particularly motivated by the observation that the large peak in the Raman spectrum of B_2O_3 glass at 806 cm^{-1} is one of the strongest pieces of evidence for the existence of boroxol rings.

Verhoef and den Hartog [48, 49] performed MD simulations of B_2O_3 glass. Although their structures comprised only BO_3 triangles without boroxol groups, they concluded that the vibrational modes of adjacent BO_3 triangles are decoupled sufficiently and a local breathing mode can occur; indeed the peak at 806 cm^{-1} in the experimental Raman spectra was assigned to such a breathing mode of three oxygen atoms within each of the BO_3 triangles.

In contrast, Bronswijk and Strijks [50] compared the experimental Raman spectrum of vitreous B_2O_3 with that of crystalline B_2O_3. They concluded that the spectrum of crystalline B_2O_3 does not show a strong, sharp and polarized band around 806 cm^{-1} (see figure 10).

Since the structures discussed in the previous section contain a high percentage of boroxol rings, lattice dynamics simulations were performed for the B_2O_3-I crystal, and for B_2O_3-a and B_2O_3-d pseudo-super-crystals using potential C2 employing the GULP program [51]. Energy minimization, i.e. adjustment of unit cell dimensions and internal

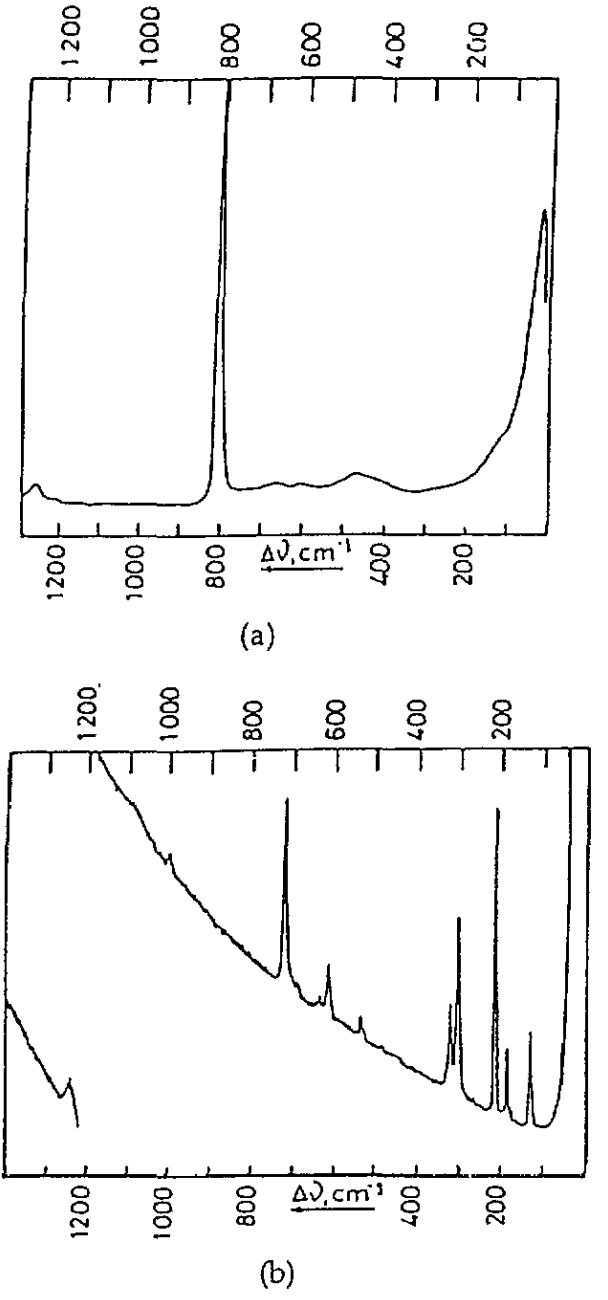

Figure 10. Experimental Raman spectra [50] for (a) vitreous B_2O_3 and (b) crystalline B_2O_3-I.

atomic coordinates, had already been performed, following which the vibrational frequencies could be calculated by diagonalizing the dynamical matrix (i.e. the matrix of the second derivatives of energy with respect to atomic coordinates) [5]. In addition, we employ the quasi-harmonic approximation which assumes that the vibrational motion in the solid is comprised of independent quantized harmonic oscillators whose frequencies vary with cell

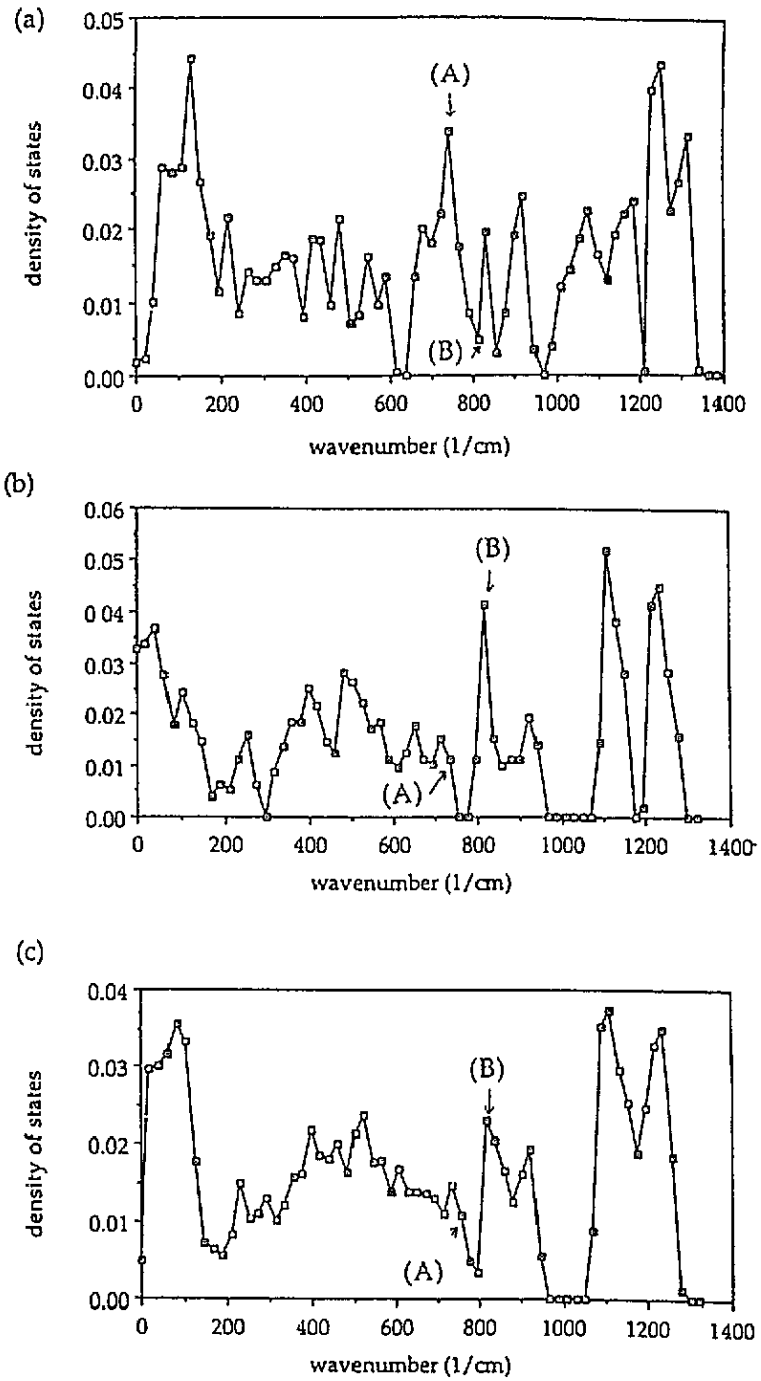

Figure 11. Calculated densities of states for (a) crystalline B_2O_3-I, (b) pseudo-super-crystal B_2O_3-a and (c) pseudo-super-crystal B_2O_3-d. (See the text for (A), (B) and (C).)

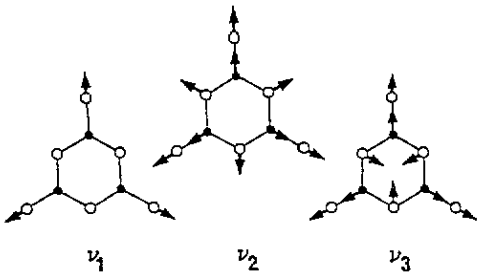

Figure 12. Symmetric vibrational modes of the 'free' metaboric anion, $B_3O_6^{3-}$. All three are Raman active and polarized.

volume [52]. This assumption allows us to calculate the frequencies at the finite temperature albeit approximately and without explicit inclusion of anharmonic effects. The calculated vibrational densities of states at 300 K are shown in figure 11.

We note first that in the spectrum of B_2O_3-I, there is a sharp peak at around 750 cm^{-1} (see the position A in figure 10(a)). It can be assigned to a bending mode in the chain structure [53], and is close to the experimental wavenumber of 720 cm^{-1}. There is no peak at 806 cm^{-1}. However, in the spectrum of B_2O_3-a, the peak at ~750 cm^{-1} disappears being replaced by a new peak at ~820 cm^{-1} (see position B in figure 10(b)), which can be assigned to the breathing mode of B_3O_6 (ν_2; see figure 12), and is close to the experimental wavenumber 806 cm^{-1}. In the spectrum of B_2O_3-d, which may be closest to the vitreous B_2O_3, there is no peak at around 750 cm^{-1}, although the structure includes BO_3 units. It shows the peak at ~820 cm^{-1}, although it is a little weaker than in the case of B_2O_3-a.

These results therefore support the hypothesis that the peak at 806 cm^{-1} in the experimental Raman spectrum in vitreous B_2O_3 can be assigned to the breathing mode of B_3O_6 units, although there are two remaining problems. The first is that the potential used (C2) was not adjusted in order to reproduce the vibrational frequencies and there is therefore a small offset in the calculated wavenumber. Secondly the structure of the pseudo-super-crystal (B_2O_3-d) must of course differ from the vitreous structure of B_2O_3. However, even if this structure were more distorted, its vibrational properties should not be markedly different, as long as there is the same fraction of boroxol rings in the structure.

8. Conclusions and summary

Our LP fitting method, which has been applied to crystals and molecular clusters of B_2O_3, has yielded several sets of potentials which can reproduce crystal structures or molecular structures.

We found first that it is essential to employ a partial charge model with a B–O Morse potential and a B–O–B bond-bending, three-body term in order to reproduce both crystal structures accurately. Moreover, to reproduce the order of energies in different phases, new potentials (C1 and C2), which depend on the coordination number around the oxygen atoms have been developed. When we compare the 'molecular' potentials with the 'crystalline' potentials, both potential sets failed when applied to both the crystal and molecular structures simultaneously. The results also showed that different values for the B–O Morse potential and the force constant for B–O–B were derived for the crystal and molecular states in a manner which can be understood in terms of changes in the degree of ionic bonding

Finally, several new possible polymorphs of B_2O_3 were obtained by performing static lattice simulations using potential C2, which can reproduce not only the structures but also the order of the lattice energies of B_2O_3 crystals. B_2O_3-d is the first structural model for

the basic unit of vitreous B_2O_3, which can reproduce not only the B–O bond lengths and the B–O–B bond angles, but also the density, with 75% of boron atoms in boroxol rings. The lattice dynamic simulations using this structure (and potential C2) also showed that the peak of the experimental Raman peak at 806 cm^{-1} can be assigned to the breathing mode of the boroxol rings. The important feature in this structure is thought to be the interlocking three-dimensional networks with two or three BO_3 units connecting the B_3O_6 units. More extensive 'computer synthesis' will enable us to obtain further possible candidates for polymorphs and vitreous structures. The subsequent paper in this series will explore the generation of structures for vitreous B_2O_3 using MD techniques.

Acknowledgment

We gratefully acknowledge many useful discussions with Dr J D Gale.

Appendix. Periodic *ab initio* Hartree–Fock calculations

Table A1. Potential energies with different lattice parameters for B_2O_3-I and B_2O_3-II. All energies are relative values to the energy in the experimental structure. v, a, b and c indicate cell volume and three lattice constants. Suffix 0 indicates an experimentally observed value. @ indicates a minimum point.

	B_2O_3-I δE (eV/B_2O_3)	B_2O_3-II δE (eV/B_2O_3)
(1) $(v/v_0)^{1/3}$		
1.020	+0.0709	
1.010	+0.0056	−0.0058
1.005	−0.0052@	−0.0119@
1.000	0.0	0.0
0.995	+0.0209	+0.0271
0.990	+0.0570	+0.0744
0.980	+0.1799	
(2) a/a_0		
1.02	+0.0371	−0.0179
1.01	+0.0005	−0.0197@
1.00	0.0@	0.0
0.99	+0.0349	+0.0419
(3) b/b_0		
1.02		+0.0137
1.01		−0.0001@
1.00		0.0
0.98		+0.0431
(4) c/c_0		
1.02	−0.0037	+0.0269
1.01	−0.0055@	+0.0057
1.00	0.0	0.0@
0.99		+0.0351
0.98	+0.0323	

In order to calculate the *ab initio* potential energy for geometries around the stable crystal structures of B_2O_3, we employed the periodic *ab initio* Hartree–Fock code CRYSTAL-92 [30].

We used the 3-21G basis set and reoptimized the exponents of the outer shell [13, 54]. The reoptimized exponents were 0.15 and 0.40 for the boron and oxygen atom respectively. Next, the total energies were calculated, varying the lattice parameters around the experimental crystal structures of both B_2O_3. The results are given in table A1. The errors in the lattice parameters, compared with the experimentally observed values, were 1.5% for B_2O_3-I and 1.5% for B_2O_3-II [2]. Thus the calculations reproduce the corresponding experimental unit cell dimensions well for both structures. The calculated *ab initio* potential energy data were used in the LP fitting.

References

[1] Pye L D, Frechett V D and Kreidl N J ed 1978 *Borate Glasses: Structure, Properties, Applications* (New York: Plenum)
[2] Takada A 1994 *PhD Thesis* University College London
[3] Takada A, Catlow C R A, Lin J S, Price G D, Lee M H, Milman V and Payne M C 1995 *Phys. Rev.* B **51** 1447
[4] Catlow C R A and Price G D 1990 *Nature* **347** 243
[5] Catlow C R A and Mackrodt W C ed 1982 *Computer Simulation of Solids (Springer Lecture Notes in Physics 166)* (Berlin: Springer)
[6] Catlow C R A, Freeman C M, Islam M S, Jackson R A, Leslie M and Tomlinson S M 1988 *Phil. Mag.* A **58** 123
[7] Dick B G and Overhauser A W 1958 *Phys. Rev.* **112** 90
[8] Tsuneyuki S, Tsukada M and Aoki H 1988 *Phys. Rev. Lett.* **61** 869
[9] Beest B W H, Kramer G J and Santen R A 1990 *Phys. Rev. Lett.* **64** 1955
[10] Sanders M J, Leslie M and Catlow C R A 1984 *J. Chem. Soc. Chem. Commun.* 1271
[11] Purton J, Jones R, Catlow C R A and Leslie M 1993 *Phys. Chem. Minerals* **19** 392
[12] Gordon R G and Kim Y S 1972 *J. Chem. Phys.* **56** 3122
[13] Gale J D, Catlow C R A and Mackrodt W C 1992 *Modell. Simul. Mater. Sci. Eng.* **1** 73
[14] Mackrodt W C and Stewart R F 1979 *J. Phys. C: Solid State Phys.* **12** 431
[15] Price G D and Parker S C 1984 *Phys. Chem. Minerals* **10** 209
[16] Vessal B, Leslie M and Catlow C R A 1989 *Mol. Simul.* **3** 123
[17] Soules T F 1980 *J Chem. Phys.* **73** 4032
[18] Soules T F and Varshneya A K 1981 *J. Am. Ceram. Soc.* **64** 145
[19] Amini M, Mitra S K and Hockney R W 1981 *J. Phys. C: Solid State Phys.* **14** 3689
[20] Hirao K and Soga N 1985 *J. Am. Ceram. Soc.* **68** 515
[21] Inoue H, Aoki N and Yasui I 1987 *J. Am. Ceram. Soc.* **70** 622
[22] Xu Q, Kawamura K and Yokokawa T 1988 *J. Non-Cryst. Solids* **104** 261
[23] Verhoef A H and den Hartog H W 1992 *J. Non-Cryst. Solids* **146** 267
[24] Gurr G E, Montgomery P W, Knutson C D and Gorres B T 1970 *Acta Crystallogr.* B **26** 906
[25] Prewitt C T and Shannon R D 1968 *Acta Crystallogr.* B **24** 869
[26] Gale J D 1993 private communication
[27] Samsonov G V 1982 *The Oxide Handbook* (New York: IFI/Plenum)
[28] THBFIT is registered in CCP5 Program Library, available from the Daresbury Laboratory, UK.
[29] Duntzig G B 1963 *Linear Programming and Extensions* (Princeton, NJ: Princeton University Press)
[30] Pisani C, Dovesi R and Roetti C 1988 *Hartree–Fock Ab Initio Treatment of Crystalline Systems* (Berlin: Springer)
[31] Gupta A and Tosell J A 1981 *Phys. Chem. Minerals* 7 159
[32] Gupta A and Tosell J A 1983 *Am. Mineral* **68** 989
[33] Gibbs G V, Meagher E P, Newton M D and Swanson D K 1981 *Structure and bonding in Crystals* ed M O'Keefe and A Navrotsky (New York: Academic)
[34] Zhang Z G, Boisen Jr M B, Finger L W and Gibbs G V 1985 *Am. Mineral.* **70** 1238
[35] Hehre W J, Radom L, Schleyer P vR and Pople J A 1986 *Ab Initio Molecular Orbital Theory* (New York: Wiley)
[36] Zachariasen W H 1934 *Z. Kristallogr.* **88** 150
[37] Zachariasen W H 1954 *Acta Crystallogr.* **7** 305
[38] Zachariasen W H 1963 *Acta Crystallogr* **16** 385

[39] Zachariasen W H 1963 *Acta Crystallogr.* **16** 380
[40] Tazaki H 1940 *J. Hiroshima Univ.* A **10** 55
[41] Peters M C and Milberg M E 1964 *Acta Crystallogr.* **17** 229
[42] Krogh-Moe J and Ihara M 1967 *Acta Crystallogr.* **23** 427
[43] Cooper A R 1978 *Borate Glases: Structure, Properties, Applications* ed L D Pye, V D Frechett and N J Kreidl N J (New York: Plenum)
[44] Elliot S R 1978 *Phil. Mag.* B **37** 435
[45] Bell R J and Carnevale A 1981 *Phil. Mag.* B **43** 389
[46] Jellison G E Jr, Panek L W, Bray D J and Rouse G B Jr 1977 *J. Chem. Phys.* **66** 802
[47] Johnson P A V and Wright A C 1982 *J. Non-Cryst. Solids* **50** 281
[48] Verhoef A H and den Hartog H W 1991 *Radiat. Eff. Defects Solids* **119–21** 493
[49] Verhoef A H and den Hartog H W 1992 *J. Non-Cryst. Solids* **146** 267
[50] Bronswijk J P and Strijks E 1977 *J. Non-Cryst. Solids* **24** 145
[51] Gale J D 1993 private communication
[52] Parker S C and Price G D 1989 *Adv. Solid-State Chem.* **1** 295
[53] Kamitsos E I and Chryssikos G D 1991 *J. Mol. Struct.* **247** 1
[54] Nada R, Catlow C R A, Dovesi R and Pisani C 1990 *Phys. Chem. Minerals* **17** 353